Calculated Proton Uptake on Anaerobic Reduction of Cytochrome *c* Oxidase: Is the Reaction Electroneutral?†

Yifan Song, Ekaterina Michonova-Alexova, and M. R. Gunner*

Physics Department J-419, City College of New York, 138th Street and Convent Avenue, New York, New York 10031

Received October 25, 2005; Revised Manuscript Received April 17, 2006

ABSTRACT: Cytochrome *c* oxidase is a transmembrane proton pump that builds an electrochemical gradient using chemical energy from the reduction of O_2. Ionization states of all residues were calculated with Multi-Conformation Continuum Electrostatics (MCCE) in seven anaerobic oxidase redox states ranging from fully oxidized to fully reduced. One long-standing problem is how proton uptake is coupled to the reduction of the active site binuclear center (BNC). The BNC has two cofactors: heme a_3 and Cu_B. If the protein needs to maintain electroneutrality, then 2 protons will be bound when the BNC is reduced by 2 electrons in the reductive half of the reaction cycle. The effective pK_as of ionizable residues around the BNC are evaluated in *Rhodobacter sphaeroides* cytochrome *c* oxidase. At pH 7, only a hydroxide coordinated to Cu_B shifts its pK_a from below 7 to above 7 and so picks up a proton when heme a_3 and Cu_B are reduced. Glu I-286, Tyr I-288, His I-334, and a second hydroxide on heme a_3 all have pK_as above 7 in all redox states, although they have only 1.6−3.5 ΔpK units energy cost for deprotonation. Thus, at equilibrium, they are protonated and cannot serve as proton acceptors. The propionic acids near the BNC are deprotonated with pK_as well below 7. They are well stabilized in their anionic state and do not bind a proton upon BNC reduction. This suggests that electroneutrality in the BNC is not maintained during the anaerobic reduction. Proton uptake on reduction of Cu_A, heme *a*, heme a_3, and Cu_B shows ≈2.5 protons bound per 4 electrons, in agreement with prior experiments. One proton is bound by a hydroxyl group in the BNC and the rest to groups far from the BNC. The electrochemical midpoint potential (E_m) of heme *a* is calculated in the fully oxidized protein and with 1 or 2 electrons in the BNC. The E_m of heme *a* shifts down when the BNC is reduced, which agrees with prior experiments. If the BNC reduction is electroneutral, then the heme *a* E_m is independent of the BNC redox state.

Heme−copper oxidases are the terminal electron acceptors in anaerobic organisms. These transmembrane proteins reduce dioxygen and convert the released chemical energy into an electrochemical gradient, across the eukaryotic mitochondrial membrane or the bacterial cell membrane (*1*−*4*). Cytochrome *c* oxidases are the most prevalent heme−copper oxidases. In this protein 4 electrons, provided by 4 cytochromes *c*, are used to reduce dioxygen to water. The 4 protons needed to make water are taken from the negative cytoplasmic side of the membrane, adding to the electrochemical gradient. Four additional protons are pumped across the membrane (*5*). Thus, each dioxygen molecule reduced by cytochrome *c* oxidase is coupled to the transfer of 8 charges across the membrane.

The first step of electron transfer is from cytochrome *c* to Cu_A, a dicopper center in subunit II which extends beyond the membrane on the proton release side of the protein (Figure 1). After receiving the electron, Cu_A reduces the 6-coordinate, low-spin, bis-His−heme *a*, which is in the center of the membrane-embedded subunit I. Heme *a* then sequentially passes 2 electrons into the binuclear center (BNC),[1] formed by a heme with a single His ligand (heme a_3) and a Cu with three His ligands (Cu_B). The BNC and heme *a* are deeply buried in the protein, approximately 20 Å from the proton input side and 15 Å from the proton release side of the membrane.

Two channels, D and K, have been identified for protons to travel from the input side of the protein into the BNC. The D channel begins with Asp I-132 near the protein surface and ends with Glu I-286 near the BNC (*6*−*8*). The K channel begins with Glu II-101(*9*, *10*), passes Lys I-362 (*11*), and ends with Tyr I-288. Both channels are more than 20 Å long and are assumed to be filled with water (*12*−*14*). It has been suggested that the single electron reduction of the fully

† This work is supported by NIH Grant RO1-GM64540.

* To whom correspondence should be addressed. Telephone: 212-650-5557. Fax: 212-650-6940. E-mail: gunner@sci.ccny.cuny.edu.

[1] Abbreviations: BNC, binuclear center containing heme a_3 and Cu_B and their axial ligands; pK'_7, in situ pK_a of a site calculated with a mean field approximation (all other protein residue and cofactor ionization and conformation states fixed in their Boltzmann distribution at pH 7); ΔG_7, free energy of ionization of a group at pH 7 obtained from pK'_7; p$K_{a,sol}$, pK_a of base or acidic group in aqueous solution; $E_{m,sol}$, electrochemical midpoint potential (E_m) of a model for the redox cofactor in aqueous solution; MCCE, Multi-Conformation Continuum Electrostatics. Key for oxidase redox states (cofactors listed in the order Cu_A, heme *a*, heme a_3, and Cu_B): O, oxidized; R, reduced; O state (OOOO), all oxidized; E state (OOOR), Cu_B reduced; R state (OORR), heme a_3 and Cu_B reduced. Aerobic states: A state, OORR state with oxygen bound; P_R state, after oxygen is reduced [heme a_3(IV)═O^{2-}, Cu_B(II)−OH^-, and deprotonated neutral Tyr I-288 radical state]; F state [heme a_3(IV)═O^{2-}, Cu_B(II)−OH^-, and protonated neutral Tyr I-288]. The propionic acids are designated A and D as found in the PDB structure file. The IUPAC nomenclature calls them respectively propionate D and C.

10.1021/bi052183d CCC: $33.50
Published on Web 06/10/2006

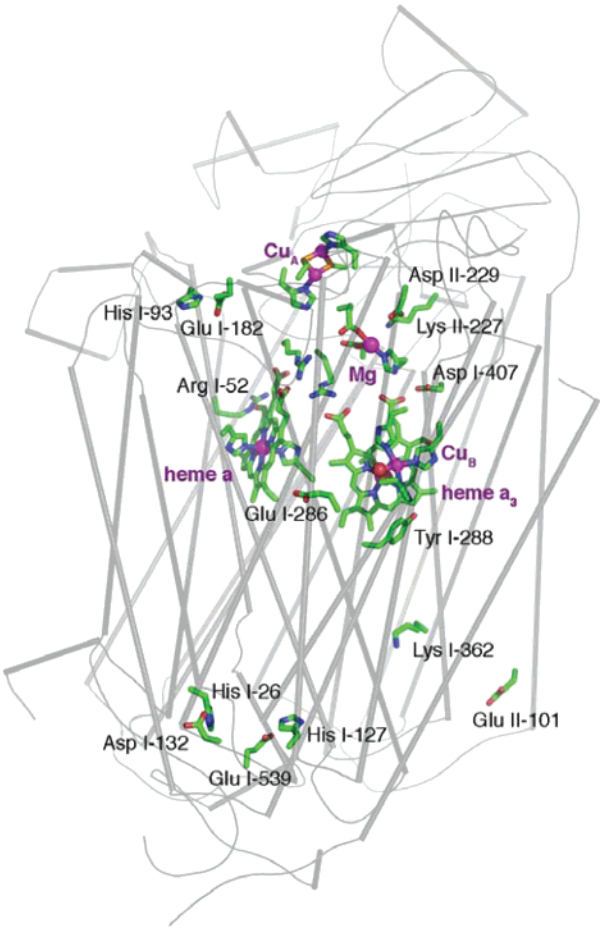

FIGURE 1: *Rb. sphaeroides* cytochrome *c* oxidase (PDB code 1M56). Backbone trace of subunits I and II. Subunits III and IV used in the calculations are not shown. Ionizable residues contributing to proton uptake or those on the proton transfer pathway are shown. Bound ions are shown as spheres. Cofactor metals are in purple and water bound to Cu_B is in red. Heme a_3 and Cu_B make up the binuclear center (BNC).

oxidized oxidase is coupled to proton uptake via the K channel (*7*, *15*−*17*) and that the second reduction is coupled to proton uptake via either the D (*7*) or K channel (*18*).

Electron transfer through oxidase changes the charge state of the redox cofactors. The favorable charge−dipole interaction of a charge with water, referred to as the solvation (reaction field or Born) energy, strongly stabilizes ionized states in water (*19*−*22*). If the charge is buried in the protein, then this favorable interaction is reduced. Consequently, the loss of solvation energy always shifts reaction equilibria in a protein, favoring states with the smaller net charge. The reduced Cu_A, heme *a*, and heme a_3 have a charge of 0, and there is a +1 on the reduced Cu_B. Cofactor oxidation in the protein, which increases the positive charge, is destabilized relative to the same redox reaction in aqueous solution by the solvation energy loss. Removal from water also shifts the pK_as of the surrounding acids and bases to favor their neutral forms. However, pairwise interactions with nearby charged groups or dipoles can stabilize buried charged residues and cofactors, compensating for the loss of solvation energy (*23*). The final in situ cofactor E_ms and residue pK_as reflect the relative contribution of these different terms. Significant perturbations, either stabilizing or destabilizing the charged forms, are well-known within proteins. For example, bis-His−hemes have E_ms ranging from −410 to +360 mV, exhibiting the ability of the protein to modify the chemical properties of buried groups. The E_m shifts for hemes with the same ligand have been shown to be caused by differences in the heme electrostatic environment within the protein (*24*−*28*).

It has been proposed that in the anoxygenic reductive half of the reaction cycle, when 2 electrons are transferred to the fully oxidized enzyme reducing heme a_3 and Cu_B, 2 protons are bound near the BNC (*29*−*31*). This requires two groups with in situ pK_as below the ambient pH in the oxidized enzyme, allowing them to be potential proton acceptors. Then when the cofactors are reduced, their pK_as would need to shift to be higher than the solution pH so each can bind a proton. If there is tight coupling between proton and electron transfers, the reaction would be electroneutral, ensuring that the oxidized and reduced BNC complexes have the same net charge. There have been several proposed proton acceptors including a hydroxide bound to Cu_B (*29*, *32*, *33*) or heme a_3 (*34*), the heme a_3 propionic acids (*12*, *29*, *35*−*37*), or one of the His ligands of Cu_B (*38*−*40*).

Various computational techniques have been used to study cytochrome *c* oxidase. Continuum electrostatics calculations carried out on the *Paracoccus denitrificans* (*33*) and bovine oxidase (*39*, *41*, *42*) showed ionization changes and long-range coupling between the BNC and the distant residues (*33*). Density functional theory (DFT) calculations have analyzed the energetics of the oxygen bond splitting reaction (*43*, *44*) and proton and electron affinities of the BNC cofactors and nearby residues (*45*). Molecular dynamics (MD) simulations have studied the behavior of water and polar residues in both the proton uptake channels and the cavities near heme *a* and the BNC (*13*, *14*, *46*). Computations have also suggested that the movements of Glu I-286 (*47*), water (*12*, *48*) near the BNC, and Thr 359 (*49*) play a role in proton pumping. The electrostatics and DFT calculations have suggested that a hydroxyl group in the BNC (*33*), the heme propionic acids (*45*), and/or a His ligand to Cu_B (*39*, *40*) contribute to the proton uptake.

MCCE (Multi-Conformation Continuum Electrostatics) calculates the shift in E_m and pK_a induced by the protein (*27*, *50*−*52*). Given measured aqueous pK_as and E_ms (p$K_{a,sol}$ and $E_{m,sol}$) for acidic and basic groups and redox cofactors, MCCE provides these values in the protein. The program is able to calculate pK_as for amino acids (*51*), heme propionates (*27*), hydroxides ligated to hemes (*53*), and E_ms for hemes in a variety of cytochromes (*25*, *27*) through benchmark calculations on simpler proteins. Prior studies on photosynthetic reaction centers (*52*, *54*, *55*), bacteriorhodopsin (*56*), and quinol:fumarate reductase (*57*) show that MCCE provides a good match to experimental values for cofactor E_ms and both cofactor and amino acid pK_as in large transmembrane proteins.

In the work presented here, MCCE was used to calculate proton uptake during the individual stages of anaerobic reduction of *Rhodobacter sphaeroides* cytochrome *c* oxidase. The in situ pK_as and proton uptake were determined for all residues. The stoichiometry of proton uptake for anaerobic reduction of the protein (*18*, *58*, *59*) and the E_m of heme *a* with the BNC cofactors in different ionization states (*31*, *60*−*62*) were computed by MCCE and compared to published experiments. There have been a variety of attempts

to measure the proton uptake occurring at specific steps of the reaction cycle (*18*, *58*, *59*). There is disagreement among the reported estimates for the stoichiometry for the first two reductive steps (*18*, *31*, *58*, *59*, *63*, *64*). The main focus of the work reported here is to determine, given the structure of the *Rb. sphaeroides* oxidase, the residues near the BNC whose equilibrium ionization states allow them to couple proton uptake to cofactor reduction and to determine if there are two proton acceptors to keep BNC reduction electroneutral.

METHODS

Subunits I−IV of the first model of the *Rb. sphaeroides* cytochrome *c* oxidase structure in the PDB file 1M56 (*65*) are analyzed with MCCE. Water molecules are removed and the internal cavities treated as a high dielectric space in the electrostatics calculation. A 32 Å slab of neutral atoms is added to provide a low dielectric membrane, with the slab position optimized to bury the fewest surface ionizable residues using the program IPECE (*56*). Buried lipids are removed.

Residue ionization is calculated with Multi-Conformation Continuum Electrostatics (MCCE2.0) (*50*, *51*). The standard MCCE subroutine is used for all amino acids and the heme propionic acids (manuscript in preparation, www.sci.ccny-.cuny.edu/∼mcce). Additional side chain rotamers are generated in 120° increments around each rotatable bond. This generates a relatively modest number of conformers. These are then pruned, removing rotamers with Lennard-Jones clashes of >10 kcal/mol with the backbone or with itself. The remaining rotamers are chosen by a randomized packing routine, where each residue finds a conformer that does not clash with the rest of the protein. The protein is packed 5000 times, and rotamers that are occupied in >5% of the packed structures are kept (manuscript in preparation). Rotamer making and pruning are carried out without protons. After pruning, protons are placed on each rotamer, and ionization and hydroxyl conformations are created for all polar and ionizable residues. In the final model there are 5062 conformers for the 1134 residues. On average, each of the 122 ionizable residues have 20 conformers and polar residues have 5−10 conformers, while nonpolar residues have 1−4 conformers.

Look-up tables are calculated for both electrostatic and nonelelctrostatic self-energies and conformer−conformer pairwise interactions (*50*). The electrostatic pairwise interactions and reaction field (solvation) energies are calculated with a finite-difference technique to solve the Poisson−Boltzmann equation, using the program DelPhi (*66*−*68*). Amino acids are given PARSE charges and radii (*69*). Four focusing runs (*70*), each with 100^3 grids, give a final resolution of 2.0 grids/Å. The protein and a 32 Å membrane slab are given a dielectric constant (ϵ) of 4, while the surrounding water has $\epsilon = 80$ with a salt concentration of 150 mM. The Lennard-Jones interactions are calculated with AMBER parameters (*71*) with the energies divided by 4 (*50*). This rescaling is needed because the Lennard-Jones parameters are optimized with electrostatic interactions calculated with $\epsilon = 1$, while in MCCE $\epsilon = 4$ is used. A smaller Lennard-Jones repulsion is needed with $\epsilon = 4$ to ensure that hydrogen bonds have the correct distance dependence.

Possible microstates of the system are subjected to Monte Carlo sampling. A microstate is made up of one conformer for each residue, cofactor, and water. The energy of microstate n (ΔG^n) is the sum of the electrostatic and nonelectrostatic energies (*27*) defined by

$$\Delta G^n = \sum_{i=1}^{M} \delta_i \{[2.3 m_i k_b T(\mathrm{pH} - \mathrm{p}K_{\mathrm{sol},i}) + n_i F(E_h - E_{\mathrm{m,sol},i})] + (\Delta\Delta G_{\mathrm{rxn},i} + \Delta G_{\mathrm{pol},i})\} + \sum_{i=1}^{M} \delta_i \sum_{j=i+1}^{M} \delta_j [\Delta G_{ij}] \quad (1)$$

where the summation is over the total M conformers of all residues in the protein; for each conformer i, $\delta_i = 1$ if it is present in the current microstate n and 0 if it is not. Each residue has one conformer with $\delta_i = 1$ and the rest $\delta_i = 0$. In the double summation δ_i and δ_j are both 1 only when conformers i and j are from two different residues. k_bT is 0.59 kcal/mol (25.8 meV); m_i is 1 for bases, −1 for acids, and 0 for polar groups and waters. n_i is the number of electrons gained or lost compared to the ground state conformer. For example, if an oxidized conformer is defined as the ground state, it has $n_i = 0$ and the reduced conformer has $n_i = 1$; F is the Faraday constant. $\mathrm{p}K_{\mathrm{sol},i}$ is the $\mathrm{p}K_a$ and $E_{\mathrm{m,sol},i}$ the midpoint potential of the ith cofactor in solution. $\Delta\Delta G_{\mathrm{rxn},i}$ is the difference between the conformer reaction field energy in solution and in the protein (desolvation energy). $\Delta G_{\mathrm{pol},i}$ is the pairwise electrostatic and nonelectrostatic interaction of the conformer with the backbone and with side chains that have no conformational degrees of freedom. The torsion energy for each conformer is added to $\Delta G_{\mathrm{pol},i}$. ΔG_{ij} is the electrostatic and Lennard-Jones pairwise interaction between each pair of conformers in the microstate. The limits on the summation of the interconformer terms ensure that each interaction is counted once. Monte Carlo sampling establishes the Boltzmann distribution of the different conformers of each residue at 25 °C. Residue $\mathrm{p}K_a$s and E_ms are determined from the fraction group ionization in a series of Monte Carlo simulations at different pHs or E_hs (eq 1). Multiflip (*72*) between closely coupled residues is implemented (*56*). The SOFT function is not used (*51*). Four hundred million steps of Monte Carlo sampling are carried out. Each reported calculation represents the average of five Monte Carlo runs. The Monte Carlo uncertainty of the conformer occupancy is ±0.01. The uncertainty of calculated E_ms is ±4 mV and ±0.07 for $\mathrm{p}K_a$s.

MCCE calculates the shift in E_m or $\mathrm{p}K_a$ when a group is transferred from solution into the protein (*27*, *52*). Thus

$$E_m = E_{\mathrm{m,sol}} - \Delta\Delta G_{\mathrm{protein}}/nF \quad (2)$$

$$\mathrm{p}K_a = \mathrm{p}K_{\mathrm{a,sol}} - m\Delta\Delta G_{\mathrm{protein}} \quad (3)$$

where m is −1 for an acid and +1 for a base. Preferably, $E_{\mathrm{m,sol}}$ and $\mathrm{p}K_{\mathrm{a,sol}}$ are obtained from measurements in aqueous solution. $\mathrm{p}K_{\mathrm{a,sol}}$ for amino acids are taken from studies of peptides (*73*, *74*). Systematic shifts are applied to the reference reaction field energies ($\Delta\Delta G_{\mathrm{RXN,sol}}$) of the ionized form of ionizable residues on the basis of the $\mathrm{p}K_a$ benchmark studies (*51*; manuscript in preparation). The shift is 0.76 $\Delta\mathrm{p}K$ unit to Asp, 0.36 $\Delta\mathrm{p}K$ unit to Glu, 1.75 $\Delta\mathrm{p}K$ units to Arg,

0.10 Δp*K* unit to Lys, 0.67 Δp*K* unit to His, 0.59 Δp*K* unit to Tyr, 1.32 Δp*K* units to the C-terminus, and 0.41 Δp*K* unit to the N-terminus. On the basis of the pK_a and E_m studies of aquo−heme proteins (*53*), −0.74 Δp*K* unit is added to ferric hydroxyl−heme and 0.5 Δp*K* unit to ferrous water−heme. The heme propionic acids are treated as previously described with a p$K_{a,sol}$ of 4.9 (*27*). Tyr I-288 is cross-linked to His I-284. The heavy atom rotamer conformation of Tyr 288 is fixed in the position found in the crystal structure. The cross-link shifts the Tyr p$K_{a,sol}$ to 8.9 (*75*), lower than the standard Tyr p$K_{a,sol}$ of 10.2. As the Tyr−His bonded interaction is included in p$K_{a,sol}$, no additional nonbonded, pairwise interactions between these two groups are included in the calculations. The non-redox-active ions, Ca^{2+} and Mg^{2+}, are each given a charge of +2. The residues that serve as ligands to these ions are fixed in their crystal structure positions and given PARSE charges (*69*). Acidic ligands are constrained to remain ionized.

Parameters for E_m and pK_a Calculations of the Cofactors. Cu_A is a dicopper complex with eight side chain and backbone groups serving as ligands. The copper atoms and ligands are treated as a complex, and the charge distribution is obtained with Gaussian 98 (*76*). The B3LYP method (*77*) with the LANL2DZ basis set (*78*) was used, and the CHELPG (*79*) algorithm was used to fit atomic charges. This charge set is able to recover measured E_ms of the designed di-Cu−azurin and of the oxidase soluble domain from different species (manuscript in preparation).

Both heme a_3 and Cu_B have one open coordinate position to bind water or hydroxyl. Conformers are built for water−heme a_3, hydroxyl−heme a_3, water−Cu_B, and hydroxyl−Cu_B. On heme a_3, the Fe−O bond is oriented perpendicular to the porphyrin plane, and the bond length is 1.95 Å with square bipyramidal geometry (*53*). The oxygen position for Cu_B is determined by DFT optimization calculations using the B3LYP method (*77*) and LANL2DZ basis set (*78*) for an isolated cupric hydroxyl−3His−Cu complex. The C_α and C_β atoms of all His ligands and the Cu are fixed in their crystal positions during optimization. This yields a distorted tetrahedral Cu geometry. The resultant O−Cu−N_ϵ(His I-333) bond angle is 136° and the Cu−O bond length is 1.9 Å. Hydrogens are located with tetrahedral oxygen geometry and bond lengths of 0.96 Å. On each cofactor, conformers of water and of hydroxyl are created by rotating the protons by 30° around the Fe−O or Cu−O bond, yielding 12 water and 12 hydroxyl positions on each cofactor. Thus, there are 48 different conformers for heme a_3 and for Cu_B given their two ionization states each with 24 possible water or hydroxyl positions. Cu_B has an additional set of conformers described below, which include the possible ionization change of a His ligand.

The approach used here to calculate the E_ms of cofactors and pK_as of the water ligands treats the metal and their ligands as a complex. The assigned $E_{m,sol}$ and p$K_{a,sol}$ are taken from the measurements of a model system for the complex in solution. The reaction field energy is also calculated, treating the whole complex. Any nonbonded pairwise interactions among the metal and its ligands are ignored since these interactions are included in the $E_{m,sol}$ and p$K_{a,sol}$. Treating cofactors and ligands as a complex thus avoids the errors inherent in using classical electrostatics to calculate the bonding energies joining them together. However, this approach requires prior knowledge of $E_{m,sol}$ and p$K_{a,sol}$ for the desired complex.

In this study, an $E_{m,sol}$ of −120 mV is assigned to the *a*-type bis-His heme found in the heme *a* site (*28*). An *a*-type heme has an extra electron-withdrawing formyl group that favors reduction (*28*). With the same ligands, the E_m of heme *a* is 100 (*28*) to 160 (*80*, *81*) mV more positive than that of *c*-type bis-His heme microperoxidase 8 (MP8) (*82*, *83*). For calculating the pK_a of water ligands, a p$K_{a,sol}$ of 9.6 is assigned to the oxidized ferric His−aquo−heme and 10.9 for the reduced ferrous His−aquo−heme, as measured with a *c*-type MP8 heme (*86*, *87*). It is assumed that water pK_as are the same in *c*-type and *a*-type hemes because the water to be protonated is not in the porphyrin plane and so should not be influenced by the formyl group on the porphyrin edge. There are fewer measurements that can be used to model the water pK_a in the Cu_B complex. A p$K_{a,sol}$ of 9.4 is used for aquo−Cu_B(II). This is taken from measurements of a tripodal ligand tris[2-(methylamino)ethyl]amine complex (*88*, *89*), which is similar to the Cu_B complex. A measured p$K_{a,sol}$ of aquo−Cu_B(I) has not been found in the literature. It is likely to be higher than that of Cu_B(II) due to the smaller positive charge on the metal. A conservative p$K_{a,sol}$ of 9.4 will be assigned to aquo−Cu_B(I) and the effects of this choice discussed below.

A metal-centered charge set is used for heme *a*, heme a_3, and Cu_B. Hemes *a* and a_3 have a +2 or +3 charge placed on Fe and −0.5 on each N atom of the porphyrin. Cu_B has a +1 or +2 charge on Cu. PARSE charges are used for the neutral His ligands. TIP3 charges are used for water ligands. CHELPG charges for the hydroxide and a His^- are calculated in isolation with the B3LYP method using the 6-31G* basis set. The metal-centered charge distribution differs from that determined by DFT calculations for the complex where some of the metal positive charge is shifted to the ligands. A +0.3 charge is placed on the formyl group C and −0.3 on the electron-withdrawing formyl group of the *a*-type hemes. This simple metal-centered charge set has been used successfully in heme benchmark calculations for bis-His and His−aquo hemes (*25*, *27*, *53*).

It has been proposed that His I-334, a ligand to Cu_B, forms an anionic imidazolate during the reaction cycle (*39*, *40*). To calculate the pK_a of this His ligand, two approaches are used. The first is the same as used for the pK_a calculations of the BNC water ligands. Cu_B and all of its His and aquo ligands are treated as one complex. There is no experimental p$K_{a,sol}$ available for such a complex with a deprotonated imidazolate. However, a p$K_{a,sol}$ of 9.0 has been calculated with DFT for a isolated Cu_B complex with water and 3 His ligands (*40*). A conformer with ionization state H_2O−His^-−Cu_B(II) is added to compete with H_2O−His^0−Cu_B(II) and OH^-−His^0−Cu_B(II) ionization states to determine the in situ His I-334 pK_a. DFT calculations were not reported with both His^- and OH^- bound on Cu_B(II) or any pK_as with a reduced Cu_B so these states cannot be addressed by treating Cu_B as a complex with its ligands. An alternative approach allows estimation of the His pK_a in the presence of OH^-, the OH^- in the presence of His^-, and the pK_as with reduced Cu_B. Here His is treated as an isolated group separate from Cu_B with its bound water and the two other His ligands. The p$K_{a,sol}$ of the free imidazolate of 14.4 is used. The reaction field energy of the His and the smaller Cu_B complex are each calculated.

Explicit nonbonded electrostatic interactions between His or His^- and the different redox and protonation states of the smaller Cu_B complex are included. This approach has been shown to work for some heme ligands (*25*), but with a metal-centered charge, continuum electrostatics often overestimates the favorable interactions between a metal and an anionic ligand.

On the basis of a study of aquo−heme pK_as and E_ms in various proteins (*53*), the Poisson−Boltzmann continuum electrostatics calculations are found to overestimate the interactions of ferric heme a_3 with Cu_B. That study compared the energies of a positive charge near a ferric aquo−heme in a vacuum calculated with DFT and with Coulomb's law. For the neutral, ferric His−hydroxyl−heme, Coulomb's law reproduces the favorable change in the heme energy found in the DFT calculations within 10%. The correlation between the Coulomb interaction and the DFT energies has a slope of 1 and is independent of the position of the external charge. Thus, the DelPhi continuum electrostatics calculations in MCCE should provide the correct interaction energies. However, there are position-dependent systematic errors in the large, unfavorable interactions with the cationic, His−water−heme complex. While interactions with negative charges, with charges in the heme plane, such as the propionic acids, and with distant charges, such as heme *a*, are well represented by Coulomb's law, when a charge is near the face of the heme, the interactions are overestimated. Interactions with groups close to the heme also need correction in the benchmark calculations of the aquo−heme pK_as in sperm whale and *Aplysia* myoglobin, hemoglobin I, heme oxygenase 1, and horseradish peroxidase (*53*).

The interaction between heme a_3 and Cu_B is investigated with DFT calculations (see Supporting Information). Different heme a_3 and Cu_B redox states, ligand protonation states, and hydrogen positions created in MCCE are tested. The correlation between DFT and Coulomb's law interactions cannot be described by a simple scaling factor. But, these results showed that the ranking of the energies between different states of the BNC agrees in the two calculations. Thus, MCCE calculations are first carried out using uncorrected Poisson−Boltzmann (PB) interactions to find the equilibrium hydrogen positions in each BNC redox and protonation state. The DFT and Coulomb's law interactions are then calculated with the equilibrium conformations. The scaling factor required to bring the Coulomb's law interactions into agreement with the DFT calculations in a vacuum is applied to the PB interactions, and the scaled values are used in the pK_a calculations. Conformers that are not occupied in the calculations with uncorrected PB interactions are omitted in the pK_a calculations. DFT, Coulomb's law, uncorrected DelPhi PB, and interactions between heme a_3 and Cu_B used in the pK_a calculations can be found in Supportinng Information (Table S1).

Analysis of the MCCE pK_as and E_ms. In the continuum electrostatics-derived MCCE analysis, the E_m or pK_a shifts found on moving a group from solution to its position in the protein ($\Delta\Delta G_{protein}$) can be broken down as (*27*, *52*)

$$\Delta\Delta G_{protein} = (\Delta\Delta G_{rxn} + \Delta G_{pol}) + \Delta G_{res} \quad (4)$$

All terms describe how the difference in free energy of reactant and product redox or protonation state changes when the group is moved from water to protein. The differences in solvation energy ($\Delta\Delta G_{rxn}$) and electrostatic and nonelectrostatic interactions with the backbone (ΔG_{pol}) are independent of the distribution of other conformers and so are independent of pH and E_h. Interactions of the group of interest with residues having conformational flexibility (ΔG_{res}) are obtained from $\Delta\Delta G_{protein}$, given the E_m and pK_a calculated by Monte Carlo sampling (eqs 2 and 3). ΔG_{res} includes the energy of rearranging the conformers, as well as the interaction of the conformers with a site of interest (*27*, *52*).

The pK_as derived from the Monte Carlo sampling as function of pH to determine the pH where 50% of the group of interest is ionized are the appropriate value to compare to experimental pK_as (*51*). However, changes in net protein charge with pH alter the electrostatic potential at each site of interest. This yields in situ pK_as that are pH dependent; consequently, the free energy of ionization does not change with pH simply by pK_a − pH, as it would in solution. The free energy of ionization at a given pH (ΔG_{pH}) can be estimated from

$$\Delta G_{pH} = 2.3mRT(pH - pK_{a,sol}) + (\Delta\Delta G_{rxn} + \Delta G_{pol} + \Delta G^{mfe}_{res,pH}) \quad (5)$$

where $\Delta G^{mfe}_{res,pH}$ is the mean field interaction of the Boltzmann-weighted distribution of conformers of the residue of interest with the Boltzmann-weighted occupancy of all other conformers in the protein at this pH (*27*, *52*). It therefore misses the energy needed if other residues change ionization or conformation state when the site of interest changes protonation state. Thus, ΔG_{pH}, the vertical energy for changing the protonation state of a residue at pH 7, is

$$\Delta G_7 = 1.36m(7 - pK'_7)\ \text{kcal/mol} = m(7 - pK'_7)\ \Delta pK\ \text{units} \quad (6)$$

where

$$pK'_7 = 7 - m(\Delta G_7/RT) \quad (7)$$

Given the protein equilibrated at pH 7, pK'_7 describes the pH where the protonation free energy would be zero (when pH = pK_a). ΔG_7 is the best measure of the stability of a given ionization state at pH 7 when the pK_a is far from 7. Thus, for residues with very high or low pK_as equilibrium ionization changes are calculated at a high or low pH where the ionization states of the rest of the protein are different than they are in the physiological pH range.

RESULTS

Ionization states of all residues in the three-subunit *Rb. sphaeroides* cytochrome *c* oxidase were calculated with Multi-Conformation Continuum Electrostatics (MCCE) in seven different anoxygenic redox states (*1*): fully oxidized (OOOO, O state), singly reduced states with Cu_A reduced (ROOO), heme *a* reduced (OROO), or Cu_B reduced (OOOR, E state), mixed valence states with heme *a* and Cu_B (ORORO) or both heme a_3 and Cu_B (OORR, R state) reduced, and the fully reduced state (RRRR). Sites where proton uptake or internal transfer is coupled to electron transfer are identified by the calculated differences in residue protonation in

Table 1: Ionization States of Key Residues[a]

A. Net charge	OOOO	ROOO	OROO	OOOR	OROR	OORR	RRRR
Release side Cluster							
His I-93	0.05	0.17	0.12	0.08	0.12	0.08	0.22
Glu I-182	-0.69	-0.37	-0.49	-0.56	-0.47	-0.54	-0.27
Total	**-0.64**	**-0.20**	**-0.37**	**-0.48**	**-0.35**	**-0.46**	**-0.05**
PropA (Heme a)	-1.00	-1.00	-1.00	-1.00	-1.00	-1.00	-0.79
BNC Cluster							
aquo-Heme a_3	0.00	0.00	0.00	-0.87	-0.09	0.00	0.00
aquo-Cu_B	-1.00	-1.00	-1.00	0.00	0.00	0.00	0.00
Glu I-286	0.00	0.00	0.00	0.00	0.00	0.00	0.00
Tyr I-288	-0.06	-0.04	0.00	0.00	0.00	0.00	0.00
Total	**-1.06**	**-1.04**	**-1.00**	**-0.87**	**-0.09**	**0.00**	**0.00**
Uptake side Cluster							
His I-127	0.31	0.29	0.48	0.37	0.44	0.44	0.50
Glu I-539	-0.62	-0.62	-0.67	-0.59	-0.64	-0.66	-0.66
Total	**-0.31**	**-0.33**	**-0.19**	**-0.22**	**-0.20**	**-0.22**	**-0.16**
Whole protein	**-4.30**	**-4.70**	**-4.80**	**-4.90**	**-4.80**	**-4.90**	**-5.80**

B. Proton uptake relative to OOOO state		ROOO	OROO	OOOR	OROR	OORR	RRRR
Release side Cluster	-	0.44	0.27	0.16	0.29	0.18	0.59
BNC Cluster	-	0.02	0.06	0.19	0.97	1.06	1.06
Uptake side Cluster	-	-0.02	0.12	0.09	0.11	0.09	0.15
Whole Protein	-	0.60	0.50	0.40	1.50	1.40	2.50

C. Step-wise proton uptake		OOOO → ROOO	ROOO → OROO	OROO → OOOR	OOOR → OROR	OROR → OORR	OORR → RRRR
Release side Cluster	-	0.44	-0.17	-0.11	0.13	-0.11	0.41
BNC Cluster	-	0.02	0.04	0.13	0.78	0.09	0.00
Uptake side Cluster	-	-0.02	0.14	-0.03	0.02	-0.02	0.06
Whole Protein	-	0.60	-0.10	-0.10	1.10	-0.10	1.10

[a] MCCE calculated ionization of key residues of *Rb. sphaeroides* cytochrome *c* oxidase in selected redox states. Charges on the aquo ligands of heme a_3 and Cu_B are shown, while the charges on the metal center and the His ligands are not included in the number. The whole protein ionization includes charges on groups not explicitly noted here. Redox states of the four cofactors are represented by the four-letter key ordered Cu_A, heme *a*, heme a_3, and Cu_B (O, oxidized; R, reduced). The A and D propionic acids are identified by their connection to the A and D rings in the PDB file.

different redox states (Table 1). In addition, pK'_7 (eq 7) was calculated for key residues, which provides the energy required to move away from the equilibrium protonation state at pH 7 (Table 2).

Residues responding to the redox state changes can be assigned to three clusters. The BNC cluster contains the hydroxyl groups coordinated to heme a_3 and/or Cu_B (*32*−*34*). In addition, the heme *a* and a_3 propionic acids (*45*), Glu I-286 (*6*−*8*), Tyr I-288, Lys I-362, and His I-334 (*38*, *39*) are essential ionizable residues in the vicinity of the BNC, which are in a position to couple proton uptake to cofactor reduction (Figure 2). On the proton release side of the protein, His I-93 and Glu I-182 form a cluster which changes ionization as the oxidase cofactors change charge (Figure 3A). The third cluster which includes His I-127 and Glu I-539 is found on the proton entry side near the D channel Asp I-132 (Figure 3B).

BNC Hydroxyl pK_as. In the absence of oxygen, Cu_B and heme a_3 each bind one water or hydroxide as their fourth and sixth ligand, respectively. To couple proton uptake to BNC reduction, the hydroxyl pK_a must be lower than the solution pH in the fully oxidized state and higher following reduction. The p$K_{a,sol}$ for deprotonation of an oxidized His−aquo−heme has been measured to be 9.6 (*86*), while that of an oxidized Cu(II) with 3 His ligands is estimated to be 9.4 (*88*, *89*). In the fully oxidized protein, MCCE Monte Carlo sampling places a hydroxyl on Cu_B down to a pH below 4 and a water on heme a_3 beyond pH 11. Using the Boltzmann-sampled ionization states of all other residues at pH 7 (Table 1), the pK'_7 of −9.4 for aquo−Cu_B indicates that 16.4 Δp*K* units (22.3 kcal/mol) are needed to protonate the hydroxyl at pH 7 (eq 6, Table 2). The heme a_3 pK'_7 is 10.7, indicating that the cost of removing a proton from this water is 3.7 Δp*K* units (5.0 kcal/mol).

The factors that determine pK'_7 can be analyzed using eq 4 (Table 3). The oxidized hydroxyl−Cu_B has a net charge of +1. When a water is bound, its charge is +2. The oxidized hydroxyl−heme a_3 has a net charge 0, and it is +1 when a water is bound. The larger charge means that the water complexes lose more solvation energy ($\Delta\Delta G_{rxn}$) than the hydroxyl complexes when they are moved into the protein. The difference stabilizes the hydroxyl form, lowering the in situ aquo−cofactor pK'_7. The $\Delta\Delta G_{rxn}$ lowers the heme a_3 pK'_7 by only 3.9 pH units, while it destabilizes the water−Cu_B by 14.7 Δp*K* units (Table 3). The favorable interaction of each hydroxyl with the positive charge on the other BNC metal center lowers the pK'_7 by >10 Δp*K* units. The interaction of either hydroxyl with the rest of the protein (ΔG_{pol} and $\Delta G^{mfe}_{res,7}$) raises its pK'_7 by ≈6 Δp*K* units (Table 3). The pK'_7 of aquo−Cu_B is −9.4 when a water is bound to heme a_3 (Table 2), while the aquo−heme a_3 pK'_7 is −5.0 with water on Cu_B. As a result, at least one hydroxyl is very stable in the oxidized BNC. However, the repulsion between the two hydroxyls destabilizes the ionization of both by 15.7 Δp*K* units. This is consistent with earlier MCCE1.0 calculations on *P. denitrificans*, which also found one hydroxyl group in the BNC in the fully oxidized enzyme (*33*). Cu_B

Table 2: pK'_7 of Residues Implicated in Oxidase Activity[a]

	OOOO	ROOO	OROO	OOOR	ORORO	OORR	RRRR
BNC cluster							
aquo−heme a_3	10.7	11.1	12.4	5.9	8.4	21.5	22.6
aquo−Cu_B	−9.4	−9.1	−7.8	26.2	16.8	18.8	20.7
Glu I-286	9.7	9.5	11.3	11.2	10.6	10.9	12.8
Tyr I-288	8.6	8.8	9.8	15.7	11.3	15.6	16.9
His I-334 (a)[b]	10.3	10.9	12.0	NA	NA	NA	NA
His I-334 (b)[b]	*15.8*	*16.4*	*17.5*	*22.9*	*31.8*	*25.5*	*27.7*
PropA heme *a*	−1.7	0.0	2.1	−0.1	3.5	0.4	6.1
PropD heme *a*	−9.3	−7.7	−6.4	−7.5	−4.8	−7.3	−3.7
PropA heme a_3	−8.0	−7.2	−6.1	−4.5	−2.3	−3.9	−1.6
PropD heme a_3	−7.5	−6.6	−5.4	−3.8	−1.6	−3.6	−0.8
release side cluster							
His I-93	6.5	7.6	7.2	6.9	7.6	6.9	8.5
Glu I-182	6.3	7.3	6.9	6.7	7.3	6.7	8.1
uptake side cluster							
His I-127	7.8	7.7	8.0	8.0	8.3	8.0	8.4
Glu I-539	6.9	7.0	7.1	7.0	7.2	7.1	7.2
D and K channel residues							
Asp I-132	0.5	0.6	0.6	0.6	0.6	0.6	0.6
Lys I-362	−2.7	−2.7	−2.9	−2.1	−2.8	−2.0	−1.2
Glu II-101	2.1	2.1	2.2	2.3	2.4	2.4	2.4

[a] pK'_7 gives the effective pK_a calculated with the protein ionization and conformation states fixed at pH 7 providing the free energy of a site changing ionization at pH 7 (eqs 5 and 6). pK'_7 depends on the ionization states of other residues. $\Delta G^{mfe}_{res,7}$ is calculated with the key residue ionization states given in Table 1. [b] pK'_7 for deprotonation of His I-334 to form the anion is calculated in two ways, as described in Methods. (a) The His has a p$K_{a,sol}$ of 9.0 in the oxidized water−Cu_B complex (*40*); pK'_7 is calculated with a hydroxyl on heme a_3 and water on Cu_B in OOOO, ROOO, and OROO states. This value is used for the OOOO state in Table 4 and Figure 6. (b, in italics) The His pK_a is calculated, starting with a p$K_{a,sol}$ of 14.4 and explicit, nonbonded pairwise interactions with Cu_B and its ligands. The equilibrium state here has a hydroxyl on Cu_B in the OOOO state. This value is used for the OORR state in Figure 6.

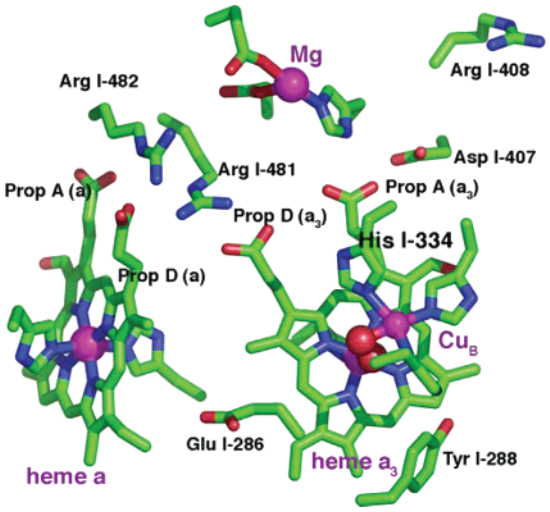

FIGURE 2: Hemes *a* and a_3, Cu_B, the Mg cluster, and nearby ionizable residues. Mg and cofactor metal atoms are shown as purple spheres. The oxygens of the BNC water ligands are in red. The heme a_3 water oxygen is behind that of Cu_B. The only labeled cofactor or ion ligand is His I-334, a Cu_B ligand whose pK_a is studied here.

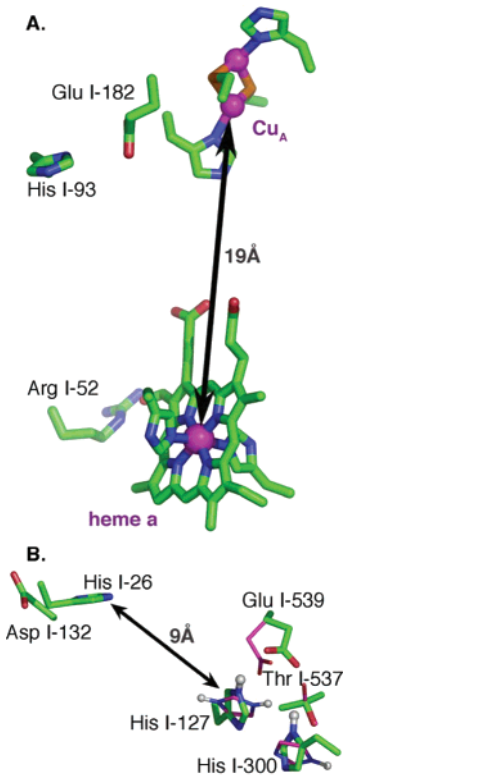

FIGURE 3: (A) Cu_A and heme *a* with their ligands, Arg 52, and the proton release side cluster, His I-93 and Glu I-182. (B) Asp I-132 and His I-26 at the D channel entrance and the proton entry side cluster, His I-127 and Glu I-539, together with His I-300 and Thr I-537. Conformational changes in the cluster when I-127 is protonated are shown with thinner purple sticks. Protons bonded to nitrogens of His I-127 and His I-300 are shown as spheres. Glu I-539 and Asp I-132 are ≈30 Å from Cu_B.

with the lower pK'_7 binds the hydroxyl, while a water is bound to heme a_3. This is in agreement with the optical absorbance measurements, which have shown a high-spin heme a_3 in oxidized cytochrome *c* oxidase (*90*). Hydroxyl−hemes are expected to be in a low-spin state (*34*, *91*), while water−hemes are generally in a high-spin state (*34*). EXAFS and ENDOR experiments support the presence of a hydroxyl−Cu_B in the oxidized enzyme (*32*).

When Cu_B is reduced forming the OOOR state, a single hydroxide is calculated to remain in the BNC. A p$K_{a,sol}$ for an aquo−Cu(I) Cu_B analogue is not found in the literature. The reduced Cu_B, with its smaller charge, should have a higher aquo−heme pK_a than the Cu(II) complex. The calculation shows that, even leaving the p$K_{a,sol}$ for the reduced hydroxyl−Cu_B at 9.4, the hydroxyl in the BNC shifts to the

Table 3: Energy Terms Used To Calculate pK'_7[a]

	net charge					$\Delta G^{mfe}_{res,7}$					
						OOOO		OORR		RRRR	
	reactant	product	p$K_{a,sol}$	$\Delta\Delta G_{rxn}$	$\Delta\Delta G_{pol}$	BNC	RES	BNC	RES	BNC	RES
ferric aquo−heme a_3	0	+1	9.6	3.9	0.4	0.2	−5.7				
ferrous aquo−heme a_3	−1	0	10.9	−10.4	0.4			4.0	−4.6	4.0	−5.7
cupric aquo−Cu_B	+1	+2	9.4	14.7	0.4	10.0	−6.3				
cuprous aquo−Cu_B	0	+1	9.4	−4.7	0.4			1.1	−6.2	1.1	−8.1
Glu I-286	0	−1	4.8	6.8	0.8	−4.3	1.6	−2.7	1.2	−2.7	3.1
Tyr I-288	0	−1	8.9	10.4	0.3	−12.4	1.3	−4.8	0.7	−4.8	2.1
His I-334[b]	+2	+1	9.0	−8.5	−2.1	2.2	9.7	NA	NA	NA	NA
	0	*−1*	*14.4*	*14.0*	*−2.1*	*−20.0*	*9.7*	*−9.0*	*8.6*	*−9.0*	*10.4*
PropA heme *a*	0	−1	4.9	10.4	−5.5	−3.8	−7.7	−1.8	−7.5	−1.8	−1.8
PropD heme *a*	0	−1	4.9	9.8	−7.3	−4.3	−12.3	−2.1	−12.5	−2.2	−8.8
PropA heme a_3	0	−1	4.9	7.1	−1.3	−10.4	−8.3	−5.1	−9.6	−5.1	−7.3
PropD heme a_3	0	−1	4.9	6.5	−3.2	−9.9	−5.8	−5.2	−6.7	−5.2	−3.8
His I-93	0	+1	6.5	2.9	−0.7	0.7	−2.9	0.4	−2.9	0.4	−4.5
Glu I-182	0	−1	4.8	4.8	−2.7	−0.7	0.2	−0.4	0.2	−0.4	1.6
His I-127	0	+1	6.5	4.8	4.4	0.7	−11.3	0.3	−11.1	0.3	−11.5
Glu I-539	0	−1	4.8	6.7	−4.1	−0.5	0.0	−0.2	−0.1	−0.2	0.1
Asp I-132	0	+1	4.8	3.3	−2.9	−0.3	−4.3	−0.2	−4.4	−0.2	−4.4
Lys I-362	0	+1	10.8	10.9	−0.7	2.6	1.2	1.6	1.0	1.7	0.2
Glu II-101	0	−1	4.8	2.7	−1.2	−0.6	−3.5	−0.3	−3.6	−0.3	−3.5

[a] The net charge of the reactant and product states is given. The reference reactant state is neutral for Prop, Glu, Lys, and His and has a neutral His I-334 and a hydroxyl on heme a_3 and Cu_B. p$K_{a,sol}$: pK_a of isolated group in aqueous solution. $\Delta\Delta G_{rxn}$: double difference of desolvation (reaction field) energy $[\text{product} - \text{reactant}]_{\text{in protein}} - [\text{product} - \text{reactant}]_{\text{in water}}$. This is generally a positive, unfavorable term when the product charge is larger than that of the reactant. ΔG_{pol} and $\Delta G^{mfe}_{res,7}$: differences in electrostatic and nonelectrostatic interactions of product and reactant states with the backbone (ΔG_{pol}), with the binuclear center cofactors and their water or hydroxyl ligands (BNC $\Delta G^{mfe}_{res,7}$), and with the protein side chains and other cofactors (RES $\Delta G^{mfe}_{res,7}$). $\Delta G^{mfe}_{res,7}$ uses a mean field energy interaction with the ionization states found by MCCE sampling at pH 7 (see Table 1 for key residues). Thus, in the OOOO state there is a water on heme a_3 and a hydroxyl on Cu_B. The hydroxyl moves to heme a_3 in the OOOR state. There are no hydroxyls in the BNC in any other redox states. For example, the $\Delta G^{mfe}_{res,7}$ BNC term for ferric aquo−heme a_3 in the OOOO state is the (ferric water−heme a_3)−(ferric hydroxyl−heme a_3) interaction with the cupric hydroxyl-Cu_B, the MCCE calculated equilibrium state for Cu_B. The interaction of the ferric water−heme and each of the Cu_B states is reduced as shown in Supporting Information (see Methods and ref *53*). [b] pK'_7 of His I-334 deprotonation is calculated in two ways, as described in Methods. The top entry uses a Cu(II)−water−His complex. This does not allow calculations with a hydroxyl on Cu(II) or any Cu(I) states. The BNC interactions are with hydroxyl−heme a_3 and its ligands only. In the bottom entry, the BNC $\Delta G^{mfe}_{res,7}$ term includes the nonbonded interactions of the Cu, the other two Cu_B His, and its aquo ligands, as well as heme a_3 with His I-334.

oxidized heme a_3. The desolvation penalty, which strongly destabilizes the water−Cu_B(II), now favors water−Cu_B(I) (Table 3). Although the reduced water−Cu_B(I) complex has the larger net charge, the hydroxyl complex has a large dipole moment and more reaction field energy in water. The pK'_7 of hydroxyl−Cu_B is 12.5 with water on the oxidized heme a_3, while the aquo−heme a_3 pK'_7 is 5.9 with water on the reduced Cu_B (Table 2). As in the fully oxidized protein, the mutual repulsion of the two hydroxyls means that only one will be found. Thus, there is little proton uptake into the BNC on the reduction of Cu_B, but the hydroxide migrates from Cu_B to heme a_3.

In the ORORstate, the aquo−heme a_3 pK'_7 shifts up to 8.4 (Table 2). Hence, a proton will be taken into the BNC at pH 7 coupled to the reduction of heme *a* if Cu_B is already reduced. The change in pK'_7 from the OOOR to ORORstate is due to the aquo−heme a_3 interaction with the neutral, reduced heme *a* being 2.5 Δp*K* units smaller than it is with the cationic, oxidized heme. After 2 electrons enter the BNC to form the R (OORR) intermediate, the aquo−cofactor's pK_as are greater than 7 so both remain protonated as calculated previously (*33*). This result agrees with experiments that show little proton release at pH 7 when CO is photolyzed off the mixed valence complex, initiating back-electron transfer moving from the OORR to ORORstate (*34*). The pK_a obtained from the fractional site ionization in Monte Carlo sampling as a function of pH for aquo−heme a_3 is 8.6, in good agreement with the measured pK_a of 9 for proton release.

The pK_as of the BNC aquo−cofactors have been calculated by Siegbahn and colleagues using the hybrid density functional method (*44*). Since no other residues are allowed to change ionization, their pK_as are equivalent to pK'_7 here. In the DFT study, the pK'_7 is <-10 for the first deprotonation with 2 waters in the site and 8 when forming two hydroxides in the OOOO state. In the MCCE calculations, the pK_as are −9.4 and 10.7. Thus, both studies agree that there will be at least one hydroxyl in the BNC. But, the stability of the system with two hydroxides differs by 3 Δp*K* units. In the DFT calculations, 10% of the oxidized BNCs would have two hydroxyls, while MCCE predicts none will.

The protein is treated differently in the two simulations. MCCE includes the whole protein in the model, while the DFT calculations include only the cofactors, their ligands, the propionates, and Tyr 288. The DFT simulation region is well chosen to make the net interaction of the BNC with other parts of the protein small. The missing interactions from the rest of the protein favor the hydroxyl groups by only $\approx$1 Δp*K* unit. A more significant difference is that the DFT calculation assumes that the BNC is in a uniform medium with $\epsilon = 4$, while MCCE puts $\epsilon = 80$ into protein cavities. The high dielectric cavity stabilizes the more highly charged water−cofactor species, shifting the aquo−heme a_3's pK'_7 up by $\approx$1 pH unit and the hydroxyl−Cu_B by $\approx$5 pH units. This term destabilizes the second hydroxide in the MCCE calculations. MCCE calculations were made, eliminating the continuum water in the cavities and the interactions with parts of the protein outside of the DFT simulation region. Here

the pK'_7s are −15.1 for aquo−Cu_B as it loses the first proton and 8.3 for aquo−heme a_3 forming the second hydroxyl in the BNC, significantly closer to the DFT values. In the OOOR state there is only one stable hydroxyl in either calculation. It has a pK_a of 7.6 in the DFT calculations and 5.9 in the standard MCCE calculations. In the MCCE calculations using DFT assumptions, the extra solvation energy drops the aquo−heme a_3 pK'_7 to 5.2.

Ionization of Tyr I-288. Tyr I-288 is at the end of the K channel, hydrogen-bonded to the water on heme a_3 (Figure 2). Oxygen reduction chemistry is likely to involve a coupled electron (*92*−*94*) and proton (*75*, *95*, *96*) transfer from this Tyr to O_2. The Tyr could also serve as a proton acceptor when the BNC is reduced, if it is deprotonated in the fully oxidized state. The MCCE calculated pK_a is 8.7 (pK'_7 8.6), so it is 6% deprotonated at pH 7. The relatively high p$K_{a,sol}$ and large desolvation energy destabilize its ionization, while the BNC positive charge favors ionization (Table 3). The pK'_7 is lowered by the p$K_{a,sol}$, being 8.9, 1.3 pH units lower than a standard Tyr, because of its attachment to His I-284 (*75*). Thus, this Tyr is neutral even in the oxidized protein, but there is only a 2.2 kcal/mol penalty for forming the anion at pH 7 in the equilibrated protein with a hydroxyl on Cu_B.

Ionization of Glu I-286. Glu I-286 is an essential residue which been proposed to shuttle chemical protons from the D channel to the BNC and pumped protons to the outside at the appropriate steps in the reaction cycle (*6*−*8*). In the fully oxidized protein, Glu I-286 is calculated to be fully protonated with a pK_a of >10 (pK'_7 9.9). Despite the low p$K_{a,sol}$ of 4.8, the loss of reaction field energy destabilizes the ionized form, keeping the Glu neutral (Table 3). Nearby cavities leading to the D channel (*46*, *47*), and to heme a_3 (*12*), solvate the Glu to lower pK'_7. Interactions with the protein, mostly contributed by the oxidized BNC, further stabilize Glu^-. The balance of favorable interaction with the protein and the large desolvation energy tunes the pK'_7 so that it takes only 4 kcal/mol to deprotonate the Glu at pH 7. This puts the ionized state low enough in energy that it can serve as an intermediate in proton transfer.

Glu I-286 has been measured to have a pK_a of 9.4 in the F state (*97*). The F state with a water−Cu_B(II) and a ferryl heme a_3 [Fe(IV)═O^{2-}] has the same net charge as the water−Cu_B(II) and ferric hydroxyl−heme a_3. In the latter state, the Glu I-286 pK'_7 would be 8.9 while it is 10 for Tyr I-288. Here Glu I-286 is 3% ionized at pH 7 and becomes 50% ionized at 10.9, titrating with a shallow pH dependence in reasonable agreement with the experimental value. The calculated Tyr pK_a is much higher than its pK'_7 which is obtained at pH 7 where Glu I-286 is neutral. Unfavorable interactions with the Glu which is ionized first with increasing pH make it harder to deprotonate the Tyr. Thus, the ionization states of the Glu and Tyr are tightly coupled with an interaction energy of 2.6 ΔpK units. Once one of them is ionized, the pK_a of the other moves well above 10. The charge distribution in the BNC determines which amino acid is ionized first. In an OOOO state with a hydroxyl−heme a_3 (similar to the F state charge distribution), the pK_a for the Glu is lower than that of the Tyr. But in the lower energy OOOO state with hydroxyl−Cu_B, the Tyr has the lower pK_a.

Ionization of the Heme Propionic Acids. All of the heme propionic acids are calculated to be deprotonated in the fully oxidized state (Table 1). The propionates on the A- and D-rings (nomenclature as in the PDB file) of heme a_3, and on the D-ring of heme *a*, are close to the BNC and have been suggested to lie on the proton pumping pathway (*12*, *35*−*37*). All of the propionic acids are stabilized by the presence of Arg I-481 and I-482. Each D-ring propionate is within hydrogen-bonding distance of an Arg. The heme a_3 A-ring propionate is further stabilized by the Mg^{2+} and its ligands: His I-411, Asp I-412, and Glu II-254. Even though the net charge of the Mg cluster is 0, the propionate is closer to the Mg^{2+} than to its anionic ligands (Figure 3). A hydrogen bond from the neutral His I-411 further stabilizes the charged state. The heme *a* A-ring propionic acid is stabilized by Arg 52. The heme a_3 propionate pK'_7s remain below 0 in all of the oxidation states, despite their increasing 2−5 pH units when the BNC is reduced (Table 2). Any changes in protonation of the propionic acids would need to be coupled to movement of the adjacent Arg, as well as to reduction of the BNC (*98*). There is little difference in the propionic acid pK'_7s for OOOR and OORR states, because the second reduction of the BNC is coupled to the protonation of the hydroxide; therefore, it is electroneutral with little long-range electrostatic impact (Table 2).

The heme *a* A-ring propionic acid has a pK'_7 near physiological pH (Table 2). It remains fully ionized when the BNC is reduced (OORR). But, when the BNC and Cu_A and heme *a* are reduced (RRRR), its pK'_7 is 6.1, so it is partially protonated at pH 7 (Table 1). However, this proton binding in the fully reduced protein is to the propionate furthest from the BNC, and it is coupled to the reduction of Cu_A and heme *a*, not the BNC cofactors.

The heme a_3 A-ring propionic acid pK'_7 has also been estimated by Siegbahn and colleagues using DFT calculations (*44*). They found that in the fully oxidized protein it is 5.2, while MCCE finds it to be −8.0. This large difference is a result of the DFT calculations being centered at the BNC cofactors, locating the propionic acids at the edge of the simulation region about 8 Å from the heme iron. Arg I-481, I-482, and the Mg^{2+} complex are not included in the calculation. These groups together stabilize the acid ionization by over 13 ΔpK units. MCCE calculations with only the groups used in the DFT calculations give a pK'_7 of 6.6, in reasonable agreement with the DFT analysis. In the OOOR state, DFT calculates the propionate pK'_7 to be 11.5, while it is −4.5 in MCCE considering the whole protein and 11.4 calculated by MCCE considering only the residues included in the DFT simulations. In the OORR state, the pK'_7 is calculated to be 11.5 with DFT calculations, −3.9 with MCCE considering the whole protein, and 12.0 with MCCE considering the same residues as in the DFT calculation. Hence, the classical electrostatics calculations can reproduce the DFT pK'_7s when the same region of the protein is considered. The simple classical calculation has the advantage of being able to routinely include the whole protein.

Ionization of His I-334. His I-334, a Cu_B ligand, has also been proposed to act as a residue whose protonation state is coupled to the BNC redox state. Earlier work by Wikström suggested that this His might break its bond to Cu_B and be doubly protonated in a His shuttle (*38*). More recently, Stuchebrukhov proposed that the His becomes a fully deprotonated imidazolate, coexisting with a hydroxyl group on Cu_B in the fully oxidized state (*39*). This His^- could then serve as a second proton acceptor, keeping the BNC

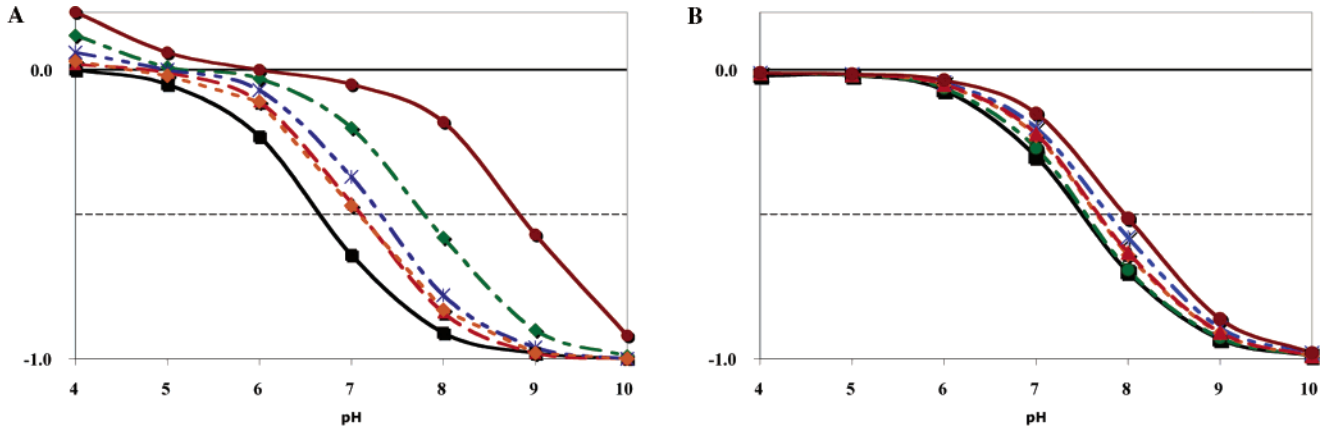

FIGURE 4: pH and redox state dependence of the net charge on clusters in cytochrome *c* oxidase. (A) Proton release cluster: His I-127 and Glu I-539. (B) Proton entry cluster: His I-93 and Glu I-182. States: (black) OOOO (6.5, 7.4), (green) ROOO (7.6, 7.4), (blue) OROO (7.2, 7.6), (orange) OOOR (6.9, 7.5), (red) OORR (6.9, 7.6), and (brown) RRRR (8.6, 8.0). The pK_a for the cluster 0 to −1 transition for the (release, entry) cluster is given in parentheses. The pK_a for the ORORO state is (7.6, 7.9) (not shown).

reduction electroneutral (*39*, *41*). A p$K_{a,sol}$ for deprotonation of a His ligand on an oxidized water−Cu_B of 9.0 was calculated with DFT (*40*). Because the His^- reduces the water−Cu_B charge, the His−water−Cu_B(II) pK_a is lowered by ≈14 ΔpK units when it is moved to a uniform medium with $\epsilon = 4$ in the MCCE calculations and by 12.3 in the DFT self-consistent reaction field calculations (*40*). This difference is likely to be due to differences in the charge distribution in the two calculations. Within the protein, cavities and the large unfavorable interactions with the heme a_3 propionates destabilize His^- (Table 3). The resultant pK'_7 of 10.3 with a hydroxyl−heme a_3 indicates that the His will remain neutral in the fully oxidized state. Earlier calculations by Stuchebrukhov using a similar model for the His−Cu_B interaction and a continuum electrostatic-based methodology similar to that found in MCCE (*99*−*103*) reported a His^- pK_a of ≈6 in the oxidized protein with a hydroxyl on Cu_B (*39*). That calculation used a p$K_{a,sol}$ for the deprotonation of the water−Cu_B−His complex of 7. With this change in p$K_{a,sol}$ the pK'_7 for His I-334 reported here would move down to 8.3. More recent calculations from the Stuchebrukhov group used a DFT-derived p$K_{a,sol}$ of 9 in aqueous calculations with (*104*) or without (*41*) a ferryl−heme a_3 included. The pK_a of His I-334 is 2.1 (*41*) or 5.4 (*104*) in the OORO state. The latter calculation includes the ferryl−heme a_3 in the reference state. In the Stuchebrukhov nomenclature R indicates any electronic state of heme a_3 with a net charge of 0 (i.e., ferrous−water, ferric−hydroxyl, or ferryl) while the O designation for Cu_B indicates that it is oxidized with a water ligand. The His I-334 pK'_7 for this state calculated by MCCE is 10.3. MCCE reports different values for both solvation energy and pairwise interactions with the other groups in the protein, contributing to the disagreement with the earlier studies (*41*, *104*).

Although the first approach is more accurate using the p$K_{a,sol}$ of the complex, the pK'_7 cannot be estimated for His deprotonation with a hydroxyl on Cu_B, because the needed p$K_{a,sol}$ is not available. To estimate this pK'_7, a second approach is used (see Methods). Here pK'_7 is estimated by starting with an isolated imidazolate p$K_{a,sol}$ of 14.4 and then including explicit nonbonded pairwise interactions between the His and Cu_B. Despite the fact that this model is likely to overstabilize the anionic ligand due to the strong interaction between the metal center and the ligand, the His pK'_7 is 15.8 (Table 3).

Protonation Changes on Residues outside the Active Site. At equilibrium, after reducing both cofactors in an initially oxidized protein, one hydroxide on a BNC cofactor has picked up a proton. In addition, other more distant residues change ionization state, contributing to the net proton uptake. The protonation of distant sites can be perturbed either by changes in the long-range electrostatic potential when the BNC is reduced or by changes in local environment if conformational rearrangements are triggered by reduction of the BNC cofactors. Electroneutral reduction of the BNC cannot yield long-range electrostatic changes. In the analysis presented here, where no backbone motions are allowed, there must be a change in the net BNC charge for proton uptake to distant residues to be coupled to electron transfer. The residues that are sensitive to small shifts in the long-range electrostatic potential are partially protonated with pK_as near 7. Two clusters, one on the proton input and one on the release side, make the largest contributions to the total proton uptake. On cofactor reduction, there are shifts in charge distribution within these clusters as well as changes in net cluster ionization.

The ionization states of His I-93 and Glu I-182, 5 Å apart on the proton output side of the protein, are coupled together (Figure 3A). At low pH (<5) 1 proton is bound with 13% $HisH^+Glu^-$ and 87% His^0GluH^0. Both microstates have a net charge of 0 and similar energies, so both are occupied. The doubly ionized state is destabilized by the desolvation penalty for the two ionized groups but stabilized by the favorable interaction between them (*105*). The cluster titrates with a pK_a of 6.7 in the OOOO state, producing a net charge of −0.64 at pH 7 (Figure 4A, Table 2). An electron on Cu_A shifts the pK_a up to 7.7, while the pK_a is 7.2 when heme *a* is reduced. The pK_a shifts of 1.0 and 0.5 lead to average protonation changes of 0.44 or 0.27 going from OOOO to ROOO or OROO states (Table 1). The pK_a shifts down to 6.9 with the first reduction of the BNC. The cluster pK_a is the same in the OOOR and OORR states, since the second reduction is coupled to the protonation of the BNC hydroxyl group and so is electroneutral. When the BNC is doubly reduced, this cluster has 0.09 more protons bound than in the fully oxidized protein. Upon the anaerobic 4-electron

reduction, the cluster binds 0.59 proton. Earlier calculations on *P. denitrificans* showed Lys II-191 (229 here) changing protonation rather than the residues shown here (*33*). This Lys was also suggested to be involved in proton release in the bovine oxidase calculations (*42*).

His I-127 and Glu I-539 form a cluster on the proton uptake side of the protein, close to Asp I-132 at the D channel entry (Figure 3B). These are far from any cofactor and more weakly coupled to cofactor redox changes than the output-side cluster. In the OOOO state, the cluster has a pK_a of 7.4, which shifts to 8.0 in the RRRR state, leading to the uptake of 0.15 proton for 4-electron reduction at pH 7.0 (Figure 4B). Conformational changes of Glu- I-539, His I-300, and Thr I-537 are calculated to be coupled to the cluster ionization changes. This reorganization of the hydrogen-bonding network could slow the cluster ionization changes, modifying the proton transfer to this cluster, which is ≈9 Å from the D channel entry.

Asp I-132 is at the D channel entrance (*106*). It is always ionized with a pK'_7 <1 in all oxidase redox states (Table 2). Since Asp I-132 is not deeply buried, it has a small desolvation penalty (Table 3). In addition, nearby backbone dipoles and an ionized His 26 stabilize the ionized Asp. Glu II-101 is at the K channel entrance (*9*, *10*, *33*). It is also kept ionized by a small desolvation penalty and favorable interactions with the backbone and other nearby residues including His II-96, which is ≈30% ionized at pH 7. This residue is equivalent to Glu II-78 in *P. denitrificans*, a residue that was previously calculated to become more protonated as the BNC is reduced (*33*). Lys I-362 is an essential conserved residue on the K channel (*11*). Although there are some suggestions that it is ionized (*107*), MCCE calculates it to be fully neutral with a pK'_7 <0 in all redox states. It is deeply buried and has few favorable interactions with neighboring residues or backbone dipoles that would stabilize the charged state. It is far enough from the BNC that its ionization is only moderately destabilized by the cofactor positive charges.

Net Proton Uptake on Reduction of Cytochrome c Oxidase. MCCE calculates that the reduction of Cu_A in the fully oxidized enzyme is coupled to the uptake of 0.6 proton to the proton exit cluster and a few nearby groups (Table 1). When the electron is transferred from Cu_A to heme *a*, the release side cluster loses 0.17 proton back to solution, while the uptake side cluster picks up 0.14 proton. All together, 0.5 proton is bound on reduction of heme *a* relative to the fully oxidized state. The calculations show negligible additional proton uptake as the electron is transferred from heme *a* to Cu_B.

There is a wide range of reported experimental values for the stoichiometry of proton uptake coupled to Cu_A and heme *a* reduction. Oxidation of the fully reduced oxidase with a CO ligand to heme a_3 (RRRR to OORR states) shows release of 0.3 (*63*), 0.4 (*58*), 0.6 (*59*), and 0.8 (*64*) protons in bovine and 0.8 proton in *P. denitrificans* (*18*) oxidase. However, the E_ms of Cu_A and heme *a* (*31*, *64*) vary by no more than 20 mV per pH unit. This is in better agreement with the smaller estimates of proton uptake. The proton uptake coupled to Cu_A and heme *a* reduction in a protein, with the BNC reduced, is calculated to lead to the binding of 0.9 H^+/2e^-. Almost all of the change is in the exit cluster, with a small amount in the proton input cluster. There are no changes in the BNC-associated residues moving from OORR to RRRR states. The MCCE value of 0.5 H^+/e^- means Cu_A and heme *a* would each have E_ms with a pH dependence of at least 30 mV per pH unit. The overestimation here is most probably due to the sensitivity of the His I-93 and Glu I-182 cluster to the electrostatic potential of Cu_A. This cluster binds 0.44 proton on the oxidation of Cu_A and releases 0.28 proton as the electron is transferred to the BNC.

The second reduction, forming either the ORORor OORR mixed valence states at pH 7, leads to the binding of 1 proton to the hydroxyl−heme a_3. The pK_a of the aquo−heme a_3 is 8.3 in the ORORstate; so it is ≈90% protonated. Thus, with Cu_B reduced, the reduction of heme *a*, not heme a_3, is calculated to be coupled to the proton binding into the BNC (Table 1). When the second electron is transferred from heme *a* into the BNC, there are only small changes in total protonation, in agreement with the experiments photolyzing the CO−heme a_3 bond in the mixed valence OORR state (*34*). Reduction of all four cofactors moving from the OOOO to RRRR state is coupled to the uptake of 2.5 protons (Table 1). Most of this is accounted for by the hydroxide in the BNC, proton uptake and release side clusters, and the heme *a* A-ring propionate, together with small changes on a few other distant groups. This is in agreement with the total proton uptake of 2.4 upon full reduction, which was measured in bovine oxidase (*58*, *59*). Yet, it is smaller than a recent measurement of 3.3 H^+/4 electrons in *P. dinitrificans* (*18*).

The E_m of Heme a. MCCE has been used successfully to calculate the heme E_ms in different bis-His cytochromes (*27*). This allows the heme *a* E_m to be calculated with no free parameters. The calculated E_m of 360 mV, when the other cofactors are oxidized, is in agreement with the experimental values of 340 mV (*31*) to 430 mV (*60*). The E_m is shifted 480 mV from the $E_{m,sol}$ of −120 mV mostly by the desolvation penalty and the positive potential from the backbone amide dipoles. Although the BNC and groups such as the heme propionates, Arg I-481 and I-482, individually have a large effect on the heme E_m, these roughly cancel. Therefore, all residues lower the E_m by only 70 mV. This match between experimental and calculated E_m is obtained with all of the heme propionates ionized; despite earlier suggestions by DFT calculations that the E_m would be too low (−150 mV) without protonation of one of the heme *a* propionates (*45*). Essentially one of the propionic acid charges was removed from the DFT calculations to compensate for not including the nearby Arg in the simulation region.

The heme *a* E_m has been found to depend on the BNC redox state. It is lowered by 80−135 mV when both Cu_B and heme a_3 are reduced (*31*, *61*, *62*, *108*). In the OORR state, the E_m is calculated to be 260 mV, 100 mV lower than in the oxidized enzyme, in good agreement with experiment. Simply adding 2 electrons to the cofactors and 1 proton to the BNC hydroxide lowers the E_m by 150 mV. Proton uptake to other distant residues diminishes the E_m shift. If the BNC reduction were electroneutral with 2H^+/2e^-, the heme E_m would be independent of the BNC redox state. If there are two hydroxyls in the oxidized BNC, the heme *a* E_m is 260 mV, the same as calculated in the fully reduced BNC, which is significantly lower than measured in the oxidized protein.

The heme *a* E_m was also calculated with Arg 52 mutated to Met. This has been observed to lower the heme *a* E_m by about 260 mV in *P. denitrificans* oxidase (*108*). In MCCE with the *Rb. sphaeroides* structure, removal of the Arg charge causes the protein to bind ≈0.5 proton. About half of this is to the heme *a* A-ring propionate. The resultant heme *a* E_m with the other cofactors oxidized is calculated to be lowered by 200 mV, in reasonable agreement with experiment.

DISCUSSION

The number of protons bound at each stage of the electron transfer cycle in cytochrome *c* oxidase has been the subject of intensive study (*1*−*4*). The desolvation penalty for reducing the deeply buried BNC has been suggested to be the primary source of the tight coupling between electron and proton transfers needed for pumping in oxidase (*29*, *58*, *109*). Transferring an electron to a cofactor deep in the protein introduces a large desolvation penalty, which can be diminished by burying another charge with an opposite sign, such as a proton, nearby. Anions in the surroundings stabilize oxidation of the deeply buried cofactors, and cofactor reduction increases their pK_as to favor proton binding (Table 2). However, the large desolvation penalty can also be compensated by pairwise interactions with nearby charged groups or dipoles (*23*). Here in the equilibrium calculations on the *Rb. sphaeroides* oxidase, only one group, the hydroxyl on Cu_B, shifts its pK_a from below 7 to above 7 to pick up a proton when 2 electrons are transferred into the BNC. Similar conclusions were found in the MCCE analysis of the *P. denitrificans* structure, where only 1 proton is also taken up on formation of the R (OORR) state (*33*). Only 1 proton is needed for the O−O bond splitting chemistry of bound O_2 in the A to P_R transition (*29*, *110*, *111*). This proton and an electron are proposed to be donated by Tyr I-288, forming a hydroxyl on Cu_B and unprotonated heme a_3 ferryl species (Fe^{4+}═O^{2-}) (*75*, *92*−*96*).

At some point in the reaction cycle following O_2 bond splitting, heme a_3 and Cu_B each will have a hydroxyl ligand with a bound chemical proton (*29*). This work has shown that the stable BNC has one hydroxide and one water in the fully oxidized state, which marks the end of the oxidative phase and the beginning of the reductive phase. Thus three chemical protons would need to be bound before reaching the stabilized fully oxidized state. However, in the O state, a deprotonated Tyr I-288, a hydroxyl on heme a_3, or an anionic His- I-334 is only 1.6−3.5 ΔpK units higher than the equilibrated state. Thus, states with a second anion in the BNC may be accessible in the oxidative phase. This raises the possibility that the equilibrated O state observed in MCCE calculations is that of the stabilized "resting" (*110*, *112*) enzyme, while a fully oxidized protein with two deprotonated groups in the BNC is a higher energy, metastable state which occurs during the reaction cycle.

Relative Energy of Different BNC Ionization States. In order for a group to be a proton acceptor when the BNC is reduced, it must have a pK_a below 7 in the oxidized protein and above 7 when the cofactors are reduced. Only the hydroxyl−Cu_B satisfies the criteria for a group whose protonation state is tightly coupled to the BNC reduction (Figure 6). All propionic acid pK'_7s remain below 7 in OOOO and OORR states. The pK'_7s of His I-334, aquo−

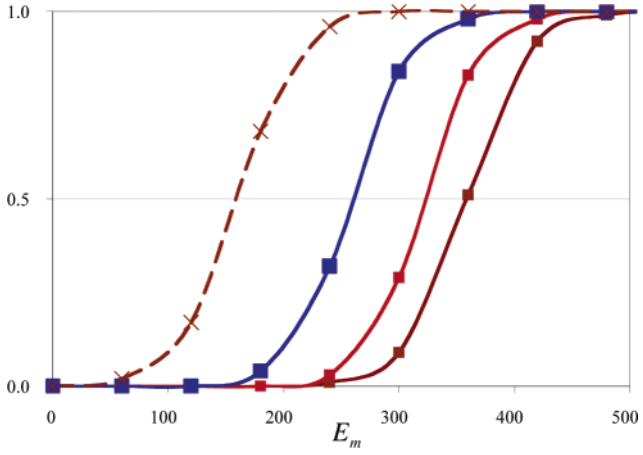

FIGURE 5: Redox titration of heme *a* with (brown) the BNC fully oxidized (E_m = 359 mV), (red) heme a_3 oxidized and Cu_B reduced (E_m = 322 mV), (blue) the BNC doubly reduced (E_m = 258 mV), and (brown dashed) the BNC fully oxidized with neutral Arg 52, as in the Arg to Met mutation (E_m = 161 mV).

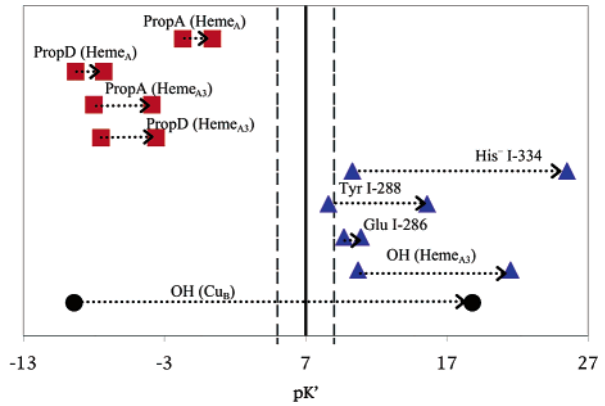

FIGURE 6: pK'_7 of the residues near the BNC in OOOO and OORR states. In all cases, pK'_7 moves to higher values in the more reduced protein. pK'_7 fixes all other residues in their lowest energy ionization state in MCCE calculations at pH 7 (Table 1). Thus, there is a hydroxyl on Cu_B in the OOOO state and no hydroxyls in the BNC in the OORR state. The four propionic acids are found to be ionized, and Tyr I-288, Glu I-286, and His I-334 are neutral in both states.

heme a_3, Glu I-286, and Tyr I-288 remain above 8. These ionization patterns are in agreement with previous calculations on *P. denitrificans* (*33*) and bovine (*39*) oxidase. Tyr I-288, with a pK_a of 8.7 (pK'_7 8.6) in the fully oxidized state, has a pK_a in the different redox states closest to what would be needed for it to be involved in proton-coupled electron transfer. The Tyr is calculated to be ≈5% deprotonated in the OOOO state; so it contributes a small amount to the proton uptake coupled to the first BNC reduction. Proton uptake via the K channel, as would likely be used to deliver protons to the Tyr, has been found experimentally on the first reduction of the BNC (*15*, *16*). The relatively low Tyr pK_a relies on its p$K_{a,sol}$ being lowered 1.3 pH units by its covalent linkage to His I-284 (*75*). With a standard p$K_{a,sol}$ of 10.2, the cost of deprotonating the Tyr would be 2.9 ΔpK units and the Tyr pK'_7 would be 9.9.

The energy of the different ionization states of the possible proton acceptors, including the hydroxyls on heme a_3 and CuB, Tyr I-288, and His I-334, can be compared in the fully oxidized *Rb. sphaeroides* cytochrome *c* oxidase (Table 4). The highest energy state is where none of these groups are

Table 4: Relative Energy of Different Protonation States of BNC Cluster Residues in the Fully Oxidized BNC[a]

state energy, pH 7 (ΔpK units)	OH^- heme a_3	OH^- Cu_B	His I-334[b]	Tyr I-288	site pK'_7[c]
neutral state					
16.4	0	0	0	0	
single anion					
0	**0**	**−1**	**0**	**0**	**−9.4**
4.4	−1	0	0	0	−5.0
10.7	0	0	0	−1	1.3
11.7	0	0	−1	0	2.3
dianionic states					
1.6	0	−1	0	−1	
3.3	−1	0	−1	0	
3.7	−1	−1	0	0	
10.1	0	0	−1	−1	

[a] Energies are relative to the state with a single OH^- on Cu_B (in bold). Ionization of all other key residues are given in Table 1. [b] Using the model for His in complex with water−Cu_B with a $pK_{a,sol}$ of 9.0 (*40*). [c] pK'_7 for groups assigned a −1 charge. This is different from that given in Table 2 since those are calculated with the ionization given in Table 1 while here the BNC residues are in the explicitly defined, nonequilibrium ionization states. 1 ΔpK unit is 1.36 kcal/mol.

ionized, and the lowest has the hydroxyl−CuB as the sole anion. The hydroxyl−heme a_3, water−CuB state is 4.4 ΔpK units higher. States with a single anion on the Tyr, or His, are at still higher energy. Thus, the lowest energy state has only one group that can serve as a proton acceptor when the BNC is reduced. The dianion hydroxyl−Cu_B, ionized Tyr state is only 1.6 ΔpK units (2.2 kcal/mol) higher, so this is the most accessible state with 2 proton acceptors. All other dianion states are at higher energy, even in the fully oxidized protein. However, the calculations do show that the single state and several dianionic states are close in energy. Additional simulations using improving methodology and comparing results from different oxidase structures and from different species will show how robust these conclusions are.

Proton binding on each reduction of the BNC has been studied experimentally. There is evidence that the stoichiometry should be $2H^+/2e^-$ upon reduction during the O to R transition, rather than 1.4, with only 1 proton bound into the BNC, as found here (Table 1). Using photoexcited ruthium bispyridyl to deliver single electrons to the *P. denitrificans* oxidase BNC, electrometric measurements of wild type and Lys I-362 to Met mutants showed that one electrometric phase is inhibited in the mutants, suggesting that the first reduction is coupled to the proton uptake via the K channel (*15*, *16*). Multiple excitation accumulates the doubly reduced enzyme, which is associated with a slower electrometric phase, attributed to a second proton uptake (*16*). Proton uptake during anaerobic reduction of the fully oxidized, CO-bound oxidase also supports a model where there are 2 protons bound on the 2-electron reduction of the BNC (*58*).

In contrast, the good match between the calculated and measured shift in the heme *a* E_m when the BNC is reduced provides evidence that there is only $1H^+/2e^-$ (*31*, *61*, *62*, *108*). If the BNC reduction is electroneutral, there is insufficient change in the long-range electrostatic potential to shift the E_m of a residue 13 Å away. In addition, the lack of proton release at pH 7 moving from the OORR to ORORstates, following flash photolysis of a bound CO (*34*), is in good agreement with the protonation of the BNC being coupled to heme *a* reduction in the OOOR state, as found here.

Assumptions and Uncertainties in the Analysis. The conclusion reported here, that there is one anionic group in the fully oxidized BNC that is strongly coupled to reduction, relies on a number of assumptions. The repulsion between the cationic oxidized water−heme a_3 and the hydroxyl−Cu_B-(II) in the fully oxidized (OOOO) and mixed valence (ORORstates has been shown, by comparison between Gaussian 98 and Coulomb's law, to be overestimated in a continuum electrostatics treatment (*53*). Using the uncorrected interactions, the pK_a of the aquo−heme a_3 is low enough that both of the BNC cofactors bind hydroxyl in the fully oxidized protein. The same correction for interactions between nearby charges is needed to obtain benchmark pK_as, in agreement with experiment for aquo−hemes in two other proteins (*53*). In addition, measurements in a model system with a Cu_B analogue inserted into myoglobin also show a surprisingly small change in the water−heme E_m when a Cu or a Zn is added, indicating a small interaction between the heme and the nearby metal (*113*).

A very simple metal-centered charge distribution is used for the cofactors in the BNC. The long-range interactions are only affected by the net charge, but local interactions are sensitive to the partial charges on individual atoms. Using Gaussian 98 charges for the hydroxyl−3His−Cu_B complex moves some of the positive charge from the copper to the His ligands, further from the hydroxyl on heme a_3. This shifts the aquo−heme a_3 pK_a up by ≈2 pH units, indicating that both of the hydroxyls are even less likely to coexist in the oxidized BNC with a more distributed charge model.

Protein cavities are filled with high dielectric continuum water, instead of explicit water in the calculations. Buried waters have been suggested to be important for oxidase activity (*12*−*14*, *46*, *48*, *114*). Earlier studies of bacteriorhodopsin have shown that the calculated pK_as are similar with either continuum or explicit water, even for active site residues (*56*). In addition, if explicit waters are not placed carefully, necessary hydrogen bonds cannot be formed to compensate for the desolvation penalty incurred by filling in the cavities with explicit waters, introducing additional errors.

Kinetic vs Thermodynamic Control of Ionization States. This analysis provides a view of the equilibrium protonation states throughout the protein in the *Rb. sphaeroides* oxidase crystal structure. The MCCE calculated pK'_7 provides the free energy needed to change the ionization of a residue, providing clues to which higher energy ionization states can be kinetically accessible. Glu I-286 and Tyr I-288 are both near the BNC at the end of the proton uptake channels. They have pK'_7s between 9 and 10 in the fully oxidized state, as well as in the P_R and F states in the oxidative phase. Hence, they are protonated at equilibrium, but they need only 2.5−4 kcal/mol for them to give up their proton. In contrast, the heme propionates on the output side of the protein have pK'_7s below 0, making it very difficult for them to be protonated without changes in the protein structure. These calculations may overestimate the cost of deprotonating the propionates since Arg motion could diminish the cost of acid protonation, raising the pK_a.

Calculations on the bacteriorhodopsin proton pump show that small changes in the structure can lead to directional

protonation shifts between residues, while each residue remains in equilibrium in the given structure. These calculations were carried out with high-resolution structures trapped in different states of the bacteriorhodopsin reaction cycle. MCCE (*56*) and MEAD (*115*) calculations with structures differing by <1 Å RMSD show changes in the active site ionization, as predicted by experiment (*116*). The agreement between the kinetic measurements and equilibrium calculations shows that the protonation states remain in equilibrium with the structure, at least for processes occurring on the slow microsecond time scale. The challenge for studies of cytochrome *c* oxidase is to find the appropriate conformational changes required to stabilize the proton transfer intermediates. Glu I-286 has been found changing conformation during an MD simulation (*117*). If this Glu can move toward the positively charged BNC, the ionized form would be stabilized, lowering the pK_a. The propionic acids are hydrogen-bonded to a pair of Arg's. If propionic acids and the Arg move apart to break the ion pair, one of the propionic acids could be protonated (*98*). His I-334 is hydrogen-bonded to two propionic acids. If the propionic acids move away from the His, the unfavorable interaction between negative imidazolate and the propionic acids would be reduced, perhaps allowing His I-334 deprotonation. Analyses of protonation states of residues equilibrated around these modified positions are ongoing.

ACKNOWLEDGMENT

We gratefully acknowledge Junjun Mao for developing and continually improving the MCCE code and Martin Wikström and Alexei Stuchebrukhov for a careful reading of the manuscript.

SUPPORTING INFORMATION AVAILABLE

A table of interactions between heme a_3 and Cu_B in different aquo protonation and cofactor redox states, values being calculated in a vacuum by Coulomb's law, by DFT using Gaussian 98, by solving the Poisson−Boltzmann equation using DelPhi in the protein, and by ($\Delta G_{PB}\Delta G_{DFT}/\Delta G_{Coulomb}$) to be used in MCCE p$K_a$ and E_m calculations. This material is available free of charge via the Internet at http://pubs.acs.org.

REFERENCES

1. Brzezinski, P. (2004) Redox-driven membrane-bound proton pumps, *Trends Biochem. Sci. 29*, 380−387.
2. Gennis, R. B. (2003) Some recent contributions of FTIR difference spectroscopy to the study of cytochrome oxidas, *FEBS Lett. 555*, 2−7.
3. Ferguson-Miller, S., and Babcock, G. T. (1996) Heme/copper terminal oxidases, *Chem. Rev. 96*, 2889−2907.
4. Wikström, M. (2004) Cytochrome *c* oxidase: 25 years of the elusive proton pump, *Biochim. Biophys. Acta 1655*, 241−247.
5. Babcock, G. T., and Wikström, M. (1992) Oxygen activation and the conservation of energy in cell respirations, *Nature 356*, 301−308.
6. Junemann, S., Meunier, B., Fisher, N., and Rich, P. R. (1999) Effects of mutation of the conserved glutamic acid-286 in subunit I of cytochrome *c* oxidase from *Rhodobacter sphaeroides*, *Biochemistry 38*, 5248−5255.
7. Wikström, M., Jasaitis, A., Backgren, C., Puustinen, A., and Verkhovsky, M. I. (2000) The role of the D- and K-pathways of proton transfer in the function of the haem-copper oxidases, *Biochim. Biophys. Acta 1459*, 514−520.
8. Ådelroth, P., Karpeforsa, M., Gildersona, G., Tomsonc, F. L., Gennis, R. B., and Brzezinski, P. (2000) Proton transfer from glutamate 286 determines the transition rates between oxygen intermediates in cytochrome *c* oxidase, *Biochim. Biophys. Acta 1459*, 533−539.
9. Branden, M., Tomson, F., Gennis, R. B., and Brzezinski, P. (2002) The entry point of the K-proton-transfer pathway in cytochrome *c* oxidase, *Biochemistry 41*, 10794−10798.
10. Tomson, F. L., Morgan, J. E., Gu, G., Barquera, B., Vygodina, T. V., and Gennis, R. B. (2003) Substitutions for glutamate 101 in subunit II of cytochrome *c* oxidase from *Rhodobacter sphaeroides* result in blocking the proton-conducting K-channel, *Biochemistry 42*, 1711−1717.
11. Junemann, S., Meunier, B., Gennis, R. B., and Rich, P. R. (1997) Effects of mutation of the conserved lysine-362 in cytochrome *c* oxidase from *Rhodobacter sphaeroides*, *Biochemistry 36*, 14456−14464.
12. Wikström, M., Verkhovsky, M. I., and Hummer, G. (2003) Water-gated mechanism of proton translocation by cytochrome *c* oxidase, *Biochim. Biophys. Acta 1604*, 61−65.
13. Zheng, X., Medvedev, D. M., Swanson, J., and Stuchebrukhov, A. A. (2003) Computer simulation of water in cytochrome *c* oxidase, *Biochim. Biophys. Acta 1557*, 99−107.
14. Olkhova, E., Hutter, M. C., Lill, M. A., Helms, V., and Michel, H. (2004) Dynamic water networks in cytochrome *c* oxidase from *Paracoccus denitrificans* investigated by molecular dynamics simulations, *Biophys. J. 86*, 1873−1889.
15. Ruitenberg, M., Kannt, A., Bamberg, E., Ludwig, B., Michel, H., and Fendler, K. (2000) Single electron reducton of the oxidized state is coupled to proton uptake via the K pathway in *Paracoccus denitrificans* cytochrome *c* oxidase, *Proc. Natl. Acad. Sci. U.S.A. 97*, 4632−4636.
16. Verkhovsky, M. I., Tuukkanen, A., Backgren, C., Puustinen, A., and Wikström, M. (2001) Charge translocation coupled to electron injection into oxidized cytochrome *c* oxidase from *Paracoccus denitrificans*, *Biochemistry 40*, 7077−7083.
17. Giuffre, A., Barone, M. C., Brunori, M., D'Itri, E., Ludwig, B., Malatesta, F., Muller, H. W., and Sarti, P. (2002) Nitric oxide reacts with the single-electron reduced active site of cytochrome *c* oxidase, *J. Biol. Chem. 277*, 22402−22406.
18. Forte, E., Scandurra, F. M., Richter, O. M. H., D'Itri, E., Sarti, P., Brunori, M., Ludwig, B., and Giuffre, A. (2004) Proton uptake upon anaerobic reduction of the *Paracoccus denitrificans* cytochrome *c* oxidase: A kinetic investigation of the K354M and D124N mutants, *Biochemistry 43*, 2957−2963.
19. Bockris, J. O. M., and Reddy, A. K. N. (1973) *Modern Electrochemistry*, Vol. 1, Plenum, New York.
20. Kassner, R. J. (1973) A theoretical model for the effects of local nonpolar heme environments on the redox potentials in cytochromes, *J. Am. Chem. Soc. 95*, 2674−2676.
21. Warshel, A., and Russell, S. T. (1984) Calculations of electrostatic interactions in biological systems and in solutions, *Q. Rev. Biophys. 17*, 283−422.
22. Rashin, A. A., and Honig, B. (1985) Reevaluation of the Born model of ion hydration, *J. Phys. Chem. 89*, 5588−5593.
23. Kim, J., Mao, J., and Gunner, M. R. (2005) Are acidic and basic groups in buried proteins predicted to be ionized?, *J. Mol. Biol. 348*, 1283−1298.
24. Churg, A. K., and Warshel, A. (1986) Control of the redox potential of cytochrome *c* and microscopic dielectric effects in proteins, *Biochemistry 25*, 1675−1681.
25. Gunner, M. R., and Honig, B. (1991) Electrostatic control of midpoint potentials in the cytochrome subunit of the *Rhodopseudomonas viridis* reaction center, *Proc. Natl. Acad. Sci. U.S.A. 88*, 9151−9155.
26. Voigt, P., and Knapp, E. W. (2003) Tuning heme redox potentials in the cytochrome *c* subunit of photosynthetic reaction centers, *J. Biol. Chem. 278*, 51993−52001.
27. Mao, J., Hauser, K., and Gunner, M. R. (2003) How cytochromes with different folds control heme redox potentials, *Biochemistry 42*, 9829−9840.
28. Reedy, C. J., and Gibney, B. R. (2004) Heme protein assemblies, *Chem. Rev. 104*, 617−649.
29. Michel, H. (1998) The mechanism of proton pumping by cytochrome *c* oxidase, *Proc. Natl. Acad. Sci. U.S.A. 95*, 12819−12824.
30. Michel, H. (1999) Cytochrome *c* oxidase: catalytic cycle and mechanisms of proton pumping—a discussion, *Biochemistry 38*, 15129−15140.

31. Moody, A. J., and Rich, P. R. (1990) The effect of pH on redox titrations of heme *a* in cyanide liganded cytochrome *c* oxidase—Experimental and modeling studies, *Biochim. Biophys. Acta 1015*, 205−215.
32. Fann, Y. C., Ahmed, I., Blackburn, N. J., Boswell, J. S., Verkhovskaya, M. L., Hoffman, B. M., and Wikström, M. (1995) Structure of Cu_B in the binuclear heme-copper center of the cytochrome aa_3-type quinol oxidase from *Bacillus subtilis*: an ENDOR and EXAFS study, *Biochemistry 34*, 10245−10255.
33. Kannt, A., Lancaster, C. R. D., and Michel, H. (1998) The coupling of electron transfer and proton translocation: electrostatic calculations on *Paracoccus denitrificans* cytochrome *c* oxidase, *Biophys. J. 74*, 708−721.
34. Branden, M., Namslauer, A., Hansson, O., Aasa, R., and Brzezinski, P. (2003) Water-hydroxide exchange reactions at the catalytic site of heme-copper oxidases, *Biochemistry 42*, 13178−13184.
35. Puustinen, A., and Wikström, M. (1999) Proton exit from the heme-copper oxidase of *Escherichia coli*, *Proc. Natl. Acad. Sci. U.S.A. 96*, 35−37.
36. Mills, D. A., and Ferguson-Miller, S. (2002) Influence of structure, pH and membrane potential on proton movement in cytochrome oxidase, *Biochim. Biophys. Acta 1555*, 96−100.
37. Behr, J., Michel, H., Mantele, W., and Hellwig, P. (2000) Functional properties of the heme propionates in cytochrome *c* oxidase from *Paracoccus denitrificans*. Evidence from FTIR difference spectroscopy and site directed mutagenesis, *Biochemistry 39*, 1356−1363.
38. Wikström, M., Bogachev, A., Finel, M., Morgan, J. E., Puustinen, A., Raitio, M., Verkhovskaya, M., and Verkhovsky, M. I. (1994) Mechanism of proton translocation by the respiratory oxidases. The histidine cycle, *Biochim. Biophys. Acta 1187*, 106−111.
39. Popovic, D. M., and Stuchebrukhov, A. A. (2004) Electrostatic study of the proton pumping mechanism in bovine heart cytochrome *c* oxidase, *J. Am. Chem. Soc. 126*, 1858−1871.
40. Quenneville, J., Popovic, D. M., and Stuchebrukhov, A. A. (2004) Redox-dependent pK_a of Cu_B histidine ligand in cytochrome *c* oxidase, *J. Phys. Chem. B 108*, 18383−18389.
41. Popovic, D. M., Quenneville, J., and Stuchebrukhov, A. A. (2005) DFT/electrostatic calculations of pK_a values in cytochrome *c* oxidase, *J. Phys. Chem. B 109*, 3616−3626.
42. Popovic, D. M., and Stuchebrukhov, A. A. (2005) Proton exit channels in bovine cytochrome *c* oxidase, *J. Phys. Chem. B 109*, 1999−2006.
43. Blomberg, M., Siegbahn, P. E. M., Babcock, G., and Wikström, M. (2000) O−O bond splitting mechanism in cytochrome oxidase, *J. Inorg. Biochem. 80*, 261−269.
44. Siegbahn, P. E. (2003) The catalytic cycle of tyrosinase: peroxide attack on the phenolate ring followed by O−O cleavage, *J. Biol. Inorg. Chem. 8*, 567−576.
45. Siegbahn, P. E. M., Blomberg, M. R. A., and Blomberg, M. L. (2003) Theoretical study of the energetics of proton pumping and oxygen reduction in cytochrome oxidase, *J. Phys. Chem. B 107*, 10946−10955.
46. Xu, J., and Voth, G. A. (2005) Computer simulation of explicit proton translocation in cytochrome *c* oxidase: The D-pathway, *Proc. Natl. Acad. Sci. U.S.A. 102*, 6795−6800.
47. Pomes, R., Hummer, G., and Wikström, M. (1999) Structure and dynamics of a proton shuttle in cytochrome *c* oxidase, *Biochim. Biophys. Acta 1365*, 255−260.
48. Seibold, S. A., Mills, D. A., Ferguson-Miller, S., and Cukier, R. I. (2005) Water chain formation and possible proton pumping routes in *Rhodobacter sphaeroides* cytochrome *c* oxidase: A molecular dynamics comparison of the wild type and R481K mutant, *Biochemistry 44*, 10475−10485.
49. Cukier, R. I. (2005) A molecular dynamics study of water chain formation in the proton-conducting K channel of cytochrome *c* oxidase, *Biochim. Biophys. Acta 1706*, 134−146.
50. Alexov, E. G., and Gunner, M. R. (1997) Incorporating protein conformational flexibility into the calculation of pH-dependent protein properties, *Biophys. J. 72*, 2075−2093.
51. Georgescu, R. E., Alexov, E. G., and Gunner, M. R. (2002) Combining conformational flexibility and continuum electrostatics for calculating pK_as in proteins, *Biophys. J. 83*, 1731−1748.
52. Zhu, Z., and Gunner, M. R. (2005) Energetics of quinone-dependent electron and proton transfers in *Rhodobacter sphaeroides* photosynthetic reaction centers, *Biochemistry 44*, 82−96.
53. Song, Y., Mao, J., and Gunner, M. R. (2006) Electrostatic environment of hemes in proteins: pK_as of hydroxyl ligands, *Biochemistry 45*, 7949−7958.
54. Gunner, M. R., Nicholls, A., and Honig, B. (1996) Electrostatic potentials in *Rhodopseudomonas viridis* reaction center: Implications for the driving force and directionality of electron transfer, *J. Phys. Chem. 100*, 4277−4291.
55. Alexov, E. G., and Gunner, M. R. (1999) Calculated protein and proton motions coupled to electron transfer: electron transfer from Q_A^- to Q_B in bacterial photosynthetic reaction centers, *Biochemistry 38*, 8253−8270.
56. Song, Y., Mao, J., and Gunner, M. R. (2003) Calculation of proton transfers in bacteriorhodopsin bR and M intermediates, *Biochemistry 42*, 9875−9888.
57. Haas, A. H., and Lancaster, C. R. (2004) Calculated coupling of transmembrane electron and proton transfer in dihemic quinol: fumarate reductase, *Biophys. J. 87*, 4298−4315.
58. Mitchell, R., and Rich, P. R. (1994) Proton uptake by cytochrome *c* oxidase on reduction and on ligand binding, *Biochim. Biophys. Acta 1186*, 19−26.
59. Forte, E., Barone, M. C., Brunori, M., Sarti, P., and Giuffre, A. (2002) Redox-linked protonation of cytochrome *c* oxidase: the effect of chloride bound to Cu_B, *Biochemistry 41*, 13046−13052.
60. Hellwig, P., Grzybek, S., Behr, J., Ludwig, B., Michel, H., and Mantele, W. (1999) Electrochemical and ultraviolet/visible/infrared spectroscopic analysis of heme a and a_3 redox reactions in the cytochrome *c* oxidase from *Paracoccus denitrificans*: separation of heme *a* and a_3 contributions and assignment of vibrational modes, *Biochemistry 38*, 1685−1694.
61. Babcock, G. T., Vickery, L. E., and Palmer, G. (1978) The electronic state of heme in cytochrome oxidase II. Oxidation-reduction potential interactions and heme iron spin state behavior observed in reductive titrations, *J. Biol. Chem. 253*, 2400−2411.
62. Carithers, R. P., and Palmer, G. (1981) Characterization of the potentiometric behavior of soluble cytochrome oxidase by magnetic circular dichroism. Evidence in support of heme-heme interaction, *J. Biol. Chem. 256*, 7967−7976.
63. Verkhovsky, M. I., Belevich, N., Morgan, J. E., and Wikström, M. (1999) Proton linkage of cytochrome a oxidoreduction in carbon monoxide-treated cytochrome *c* oxidase, *Biochim. Biophys. Acta 1412*, 184−189.
64. Capitanio, N., Capitanio, G., Minuto, M., DeNitto, E., Palese, L. L., Nicholls, P., and Papa, S. (2000) Coupling of electron transfer with proton transfer at heme a and Cu_A redox Bohr effects in cytochrome *c* oxidase, *Biochemistry 39*, 6373−6379.
65. Svensson-Ek, M., Abramson, J., Larsson, G., Tornroth, S., Brzezinski, P., and Iwata, S. (2002) The X-ray crystal structures of wild-type and EQ(I-286) mutant cytochrome *c* oxidases from *Rhodobacter sphaeroides*, *J. Mol. Biol. 321*, 329−339.
66. Nicholls, A., and Honig, B. (1991) A rapid finite difference algorithm utilizing successive over-relaxation to solve the Poisson−Boltzmann equation, *J. Comput. Chem. 12*, 435−445.
67. Bharadwaj, R., Windemuth, A., Sridharan, S., Honig, B., and Nicholls, A. (1995) The fast multipole boundary element method for molecular electrostatics: An optimal approach for large systems, *J. Comput. Chem. 16*, 898−913.
68. Rocchia, W., Alexov, E., and Honig, B. (2001) Extending the applicability of the nonlinear Poisson−Boltzmann equation: multiple dielectric constants and multivalent ions, *J. Phys. Chem. B 105*, 6507−6514.
69. Sitkoff, D., Sharp, K. A., and Honig, B. (1994) Accurate calculation of hydration free energies using macroscopic solvent models, *J. Phys. Chem. 98*, 1978−1988.
70. Gilson, M. K., and Honig, B. (1988) Calculation of the total electrostatic energy of a macromolecular system: solvation energies, binding energies, and conformational analysis, *Proteins: Struct., Funct., Genet. 4*, 7−18.
71. Cornell, W. D., Cieplak, P., Bayly, C. I., Gould, I. R., Merz, K. M., Ferguson, D. M., Spellmeyer, D. C., Fox, T., Caldwell, J. W., and Kollman, P. A. (1995) A second generation force field for the simulation of proteins, nucleic acids, and organic molecules, *J. Am. Chem. Soc. 117*, 5179−5197.
72. Beroza, P., Fredkin, D. R., Okamura, M. Y., and Feher, G. (1991) Protonation of interacting residues in a protein by a Monte Carlo method: application to lysozyme and the photosynthetic reaction center of *Rhodobacter sphaeroides*, *Proc. Natl. Acad. Sci. U.S.A. 88*, 5804−5808.
73. Richarz, R., and Wüthrich, K. (1975) Carbon-13 NMR chemical shifts of the common amino acid residues measured in aqueous

solutions of the linear tetrapeptides H-Gly-Gly-X-L-Ala-OH, *Biopolymers 17*, 2133−2141.
74. Matthew, J. B., Gurd, F. R. N., Garcia-Moreno, B., Flanagan, M. A., March, K. L., and Shire, S. J. (1985) pH-dependent processes in proteins, *CRC Crit. Rev. Biochem. 18*, 91−197.
75. McCauley, K. M., Vrtis, J. M., Dupont, J., and van der Donk, W. A. (2000) Insights into the functional role of the tyrosine-histidine linkage in cytochrome *c* oxidase, *J. Am. Chem. Soc. 122*, 2403−2404.
76. Frisch, M. J., Trucks, G. W., Schlegel, H. B., Scuseria, G. E., Robb, M. A., Cheeseman, J. R., Zakrzewski, V. G., Montgomery, J., Stratmann, R. E., Burant, J. C., Dapprich, S., Millam, J. M., Daniels, A. D., Kudin, K. N., Strain, M. C., Farkas, O., Tomasi, J., Barone, V., Cossi, M., Cammi, R., Mennucci, B., Pomelli, C., Adamo, C., Clifford, S., Ochterski, J., Petersson, G. A., Ayala, P. Y., Cui, Q., Morokuma, K., Malick, D. K., Rabuck, A. D., Raghavachari, K., Foresman, J. B., Cioslowski, J., Ortiz, J. V., Baboul, A. G., Stefanov, B. B., Liu, G., Liashenko, A., Piskorz, P., Komaromi, I., Gomperts, R., Martin, R. L., Fox, D. J., Keith, T., Al-Laham, M. A., Peng, C. Y., Nanayakkara, A., Challacombe, M., Gill, P. M. W., Johnson, B., Chen, W., Wong, M. W., Andres, J. L., Gonzalez, C., Head-Gordon, M., Replogle, E. S., and Pople, J. A. (1998) Gaussian 98, Revision A.9, Gaussian, Inc., Pittsburgh, PA.
77. Becke, A. D. (1993) Density-functional thermochemistry. 3. The role of exact exchange, *J. Chem. Phys. 98*, 5648−5652.
78. Hay, P. J., and Wadt, W. R. (1985) Ab initio effective core potentials for molecular calculations. Potentials for the transition metal atoms Sc to Hg, *J. Chem. Phys. 82*, 270−283.
79. Breneman, C. M., and Wiberg, K. B. (1990) Determining atom-centered monopoles from molecular electrostatic potentials−The need for high sampling density in formamide conformational-analysis, *J. Comput. Chem. 11*, 361−373.
80. Vanderkooi, G., and Stotz, E. (1965) Reductive alteration of heme *a* hemochromes, *J. Biol. Chem. 240*, 3418−3424.
81. Vanderkooi, G., and Stotz, E. (1966) Oxidation-reduction potentials of heme *a* hemochromes, *J. Biol. Chem. 241*, 3316−3323.
82. Battistuzzi, G., Borsari, M., Cowan, J. A., Ranieri, A., and Sola, M. (2002) Control of cytochrome *c* redox potential: axial ligation and protein environment effects, *J. Am. Chem. Soc. 124*, 5315−5324.
83. Wilson, G. S. (1974) Electrochemical studies of porphyrin redox reactions as cytochromes models, *Bioelectrochem. Bioenerg. 1*, 172−179.
84. Marques, H. M., Cukrowski, I., and Vashi, P. R. (2000) Coordination of weak field ligands by *N*-acetylmicroperoxidase-8 (NAcMP8), a ferric haempeptide from cytochrome *c*, and the influence of the axial ligand on the reduction potential of complexes of NAcMP8, *J. Chem. Soc. 2000*, 1335−1342.
85. Santucci, R., Reinhard, H., and Brunori, M. (1988) Direct electrochemistry of the undacapeptide from cytochrome *c* (microperoxidase) at a glassy carbon electrode, *J. Am. Chem. Soc. 110*, 8536−8357.
86. Munro, O. Q., and Marques, H. M. (1996) Heme-peptide models for hemoproteins. 1. Solution chemistry of *N*-acetylmicroperoxidase-8, *Inorg. Chem. 35*, 3752−3767.
87. Vashi, P. R., and Marques, H. M. (2004) The coordination of imidazole and substituted pyridines by the hemeoctapeptide *N*-acetyl-ferromicroperoxidase-8 (Fe^{II}NAcMP8), *J. Inorg. Biochem. 98*, 1471−1482.
88. Anderegg, G., and Gramlich, V. (1994) Metal complexes of bivalent cobalt, nickel, copper, zinc, and cadmium with the tripodal ligand tris[2-(dimethylamino)ethyl]amine: their stabilities and the X-ray crystal structure of its copper(T1) complex sulfate, *Helv. Chim. Acta 77*, 685−690.
89. Thaler, F., Hubbard, C. D., Heinemann, F. W., Eldik, R. v., Schindler, S., Fabian, I., Dittler-Klingemann, A. M., Hahn, F. E., and Orvig, C. (1998) Structural, spectroscopic, thermodynamic and kinetic properties of copper(II) complexes with tripodal tetraamines, *Inorg. Chem. 37*, 4022−4029.
90. Liao, G. L., and Palmer, G. (1996) The reduced minus oxidized difference spectra of cytochromes *a* and a_3, *Biochim. Biophys. Acta 1274*, 109−111.
91. Sitter, A. J., Shifflett, J. R., and Terner, J. (1988) Resonance Raman spectroscopic evidence for heme iron-hydroxide ligation in peroxidase alkaline forms, *J. Biol. Chem. 263*, 13032−13038.
92. Proshlyakov, D. A., Ogura, T., Shinzawa-Itoh, K., Yoshikawa, S., and Kitagawa, T. (1996) Resonance Raman/absorption characterization of the oxo intermediates of cytochrome *c* oxidase generated in its reaction with hydrogen peroxide: pH and H_2O_2 concentration dependence, *Biochemistry 35*, 8580−8586.
93. MacMillan, F., Kannt, A., Behr, J., Prisner, T., and Michel, H. (1999) Direct evidence for a tyrosine radical in the reaction of cytochrome *c* oxidase with hydrogen peroxide, *Biochemistry 38*, 9179−9184.
94. Proshlyakov, D. A., Pressler, M. A., Demaso, C., Leykam, J. F., Dewitt, D. L., and Babcock, G. T. (2000) Oxygen activation and reduction in respiration involvement of redox-active tyrosine 244, *Science 290*, 1588−1591.
95. Boulatov, R., Collman, J. P., Shiryaeva, I. M., and Sunderland, C. J. (2002) Functional analogues of the dioxygen reduction site in cytochrome oxidase: mechanistic aspects and possible effects of Cu_B, *J. Am. Chem. Soc. 124*, 11923−11935.
96. Cappuccio, J. A., Ayala, I., Elliott, G. I., Szundi, I., Lewis, J., Konopelski, J. P., Barry, B. A., and Einarsdottir, O. (2002) Modeling the active site of cytochrome oxidase: synthesis and characterization of a cross-linked histidine-phenol, *J. Am. Chem. Soc. 124*, 1750−1760.
97. Namslauer, A., Aagaard, A., Katsonouri, A., and Brzezinski, P. (2003) Intramolecular proton-transfer reactions in a membrane-bound proton pump: the effect of pH on the peroxy to ferryl transition in cytochrome *c* oxidase, *Biochemistry 42*, 1488−1498.
98. Wikström, M., Ribacka, C., Molin, M., Laakkonen, L., Verkhovsky, M., and Puustien, A. (2005) Gating of proton and water transfer in the respiratory enzyme cytochrome *c* oxidase, *Proc. Natl. Acad. Sci. U.S.A. 102*, 10478−10481.
99. You, T. J., and Bashford, D. (1995) Conformation and hydrogen ion titration of proteins: a continuum electrostatic model with conformational flexibility, *Biophys. J. 69*, 1721−1733.
100. Bashford, D., and Gerwert, K. (1992) Electrostatic calculations of the pK_a values of ionizable groups in bacteriorhodopsin, *J. Mol. Biol. 224*, 473−486.
101. Bashford, D., and Karplus, M. (1991) Multiple-site titration curves of proteins: An analysis of exact and approximate methods for their calculation, *J. Phys. Chem. 95*, 9556−9561.
102. Antosiewicz, J., McCammon, J. A., and Gilson, M. K. (1994) Prediction of pH-dependent properties of proteins, *J. Mol. Biol. 238*, 415−436.
103. Antosiewicz, J., McCammon, J. A., and Gilson, M. K. (1996) The determinants of pK_as in proteins, *Biochemistry 35*, 7819−7833.
104. Quenneville, J., Popovic, D. M., and Stuchebrukhov, A. A. (2006) Combined DFT and electrostatics study of the proton pumping mechanism in cytochrome *c* oxidase, *Biochim Biophys Acta* (in press).
105. Honig, B. H., and Hubble, W. L. (1984) Stability of "salt bridges" in membrane proteins, *Proc. Natl. Acad. Sci. U.S.A. 81*, 5412−5416.
106. Mills, D. A., Florens, L., Hiser, C., Qian, J., and Ferguson-Miller, S. (2000) Where is "outside" in cytochrome *c* oxidase and how and when do protons get there?, *Biochim. Biophys. Acta 1458*, 180−187.
107. Branden, M., Sigurdson, H., Namslauer, A., Gennis, R. B., Adelroth, P., and Brzezinski, P. (2001) On the role of the K-proton-transfer pathway in cytochrome *c* oxidase, *Proc. Natl. Acad. Sci. U.S.A. 98*, 5013−5018.
108. Kannt, A., Pfitzner, U., Ruitenberg, M., Hellwig, P., Ludwig, B., Mantele, W., Fendler, K., and Michel, H. (1999) Mutation of Arg-54 strongly influences heme composition and rate and directionality of electron transfer in *Paracoccus dinitrificans* cytochrome *c* oxidase, *J. Biol. Chem. 274*, 37974−37981.
109. Mitchell, R., Mitchell, P., and Rich, P. R. (1992) Protonation states of the catalytic intermediates of cytochrome *c* oxidase, *Biochim. Biophys. Acta 1101*, 188−191.
110. Wikström, M., and Verkhovsky, M. I. (2002) Proton translocation by cytochrome *c* oxidase in different phases of the catalytic cycle, *Biochim. Biophys. Acta 1555*, 128−132.
111. Brzezinski, P., and Larsson, G. (2003) Redox-driven proton pumping by heme-copper oxidases, *Biochim. Biophys. Acta 1605*, 1−13.
112. Bloch, D., Belevich, I., Jasaitis, A., Ribacka, C., Puustinen, A., Verkhovsky, M. I., and Wikström, M. (2004) The catalytic cycle of cytochrome *c* oxidase is not the sum of its two halves, *Proc. Natl. Acad. Sci. U.S.A. 101*, 529−533.
113. Zhao, X., Yeung, N., Wang, Z., Guo, Z., and Lu, Y. (2005) Effects of metal ions in the Cu_B on the redox properties of heme in heme-copper oxidases: spectroelectrochemical studies of an engineered heme-copper center in myoglobin, *Biochemistry 44*, 1210−1214.

114. Olsson, M. H., Sharma, P. K., and Warshel, A. (2005) Simulating redox coupled proton transfer in cytochrome *c* oxidase: looking for the proton bottleneck, *FEBS Lett. 579*, 2026−2034.

115. Onufriev, A., Smondyrev, A., and Bashford, D. (2003) Proton affinity changes driving unidirectional proton transport in the bacteriorhodopsin photocycle, *J. Mol. Biol. 332*, 1183−1193.

116. Balashov, S. P. (2000) Protonation reactions and their coupling in bacteriorhodopsin, *Biochim. Biophys. Acta 1460*, 75−94.

117. Hofacker, I., and Schulten, K. (1998) Oxygen and proton pathways in cytochrome *c* oxidase, *Proteins: Struct., Funct., Genet. 30*, 100−107.

BI052183D